Geophysical Journal International

Geophys. J. Int. (2015) **202,** 1–16 doi: 10.1093/gji/ggv062

GJI Marine geosciences and applied geophysics

Seismic interferometry by multidimensional deconvolution without wavefield separation

Matteo Ravasi,[1] Giovanni Meles,[1] Andrew Curtis,[1] Zara Rawlinson[2] and Liu Yikuo[1]

[1]*School of GeoSciences, The University of Edinburgh, Grant Institute, James Hutton Road, Edinburgh, EH9 3FE, UK. E-mail: M.Ravasi@sms.ed.ac.uk*
[2]*GNS Science, 1 Fairway Drive, Avalon 5010, PO Box 30-368, Lower Hutt 5040, New Zealand*

Accepted 2015 February 6. Received 2015 February 3; in original form 2014 July 30

SUMMARY

Seismic interferometry comprises a suite of methods to redatum recorded wavefields to those that would have been recorded if different sources (so-called virtual sources) had been activated. Seismic interferometry by cross-correlation has been formulated using either two-way (for full wavefields) or one-way (for directionally decomposed wavefields) representation theorems. To obtain improved Green's function estimates, the cross-correlation result can be deconvolved by a quantity that identifies the smearing of the virtual source in space and time, the so-called point-spread function. This type of interferometry, known as interferometry by multidimensional deconvolution (MDD), has so far been applied only to one-way directionally decomposed fields, requiring accurate wavefield decomposition from dual (e.g. pressure and velocity) recordings. Here we propose a form of interferometry by multidimensional deconvolution that uses full wavefields with two-way representations, and simultaneously invert for pressure and (normal) velocity Green's functions, rather than only velocity responses as for its one-way counterpart. Tests on synthetic data show that two-way MDD improves on results of interferometry by cross-correlation, and generally produces estimates of similar quality to those obtained by one-way MDD, suggesting that the preliminary decomposition into up- and downgoing components of the pressure field is not required if pressure and velocity data are jointly used in the deconvolution. We also show that constraints on the directionality of the Green's functions sought can be added directly into the MDD inversion process to further improve two-way multidimensional deconvolution. Finally, as a by-product of having pressure and particle velocity measurements, we adapt one- and two-way representation theorems to convert any particle velocity receiver into its corresponding virtual dipole/gradient source by means of MDD. Thus data recorded from standard monopolar (e.g. marine) pressure sources can be converted into data from dipolar (derivative) sources at no extra acquisition cost.

Key words: Inverse theory; Interferometry; Controlled source seismology; Body waves; Computational seismology.

INTRODUCTION

In geophysical exploration, seismic interferometry comprises a set of techniques that allow a wavefield (theoretically, a Green's function) that would propagate between two receiver locations to be synthetized, as if one receiver had been replaced by an impulsive (or transient) source, generally known as a virtual source. This is usually obtained by cross-correlation of the wavefields observed at each receiver from an enclosing boundary or distribution of energy sources (Weaver & Lobkis 2001; Campillo & Paul 2003; Curtis *et al.* 2006; Schuster 2009; Wapenaar *et al.* 2010a,b; Galetti & Curtis 2012). Various authors have derived the theory for lossless (Schuster *et al.* 2004; Wapenaar 2004; van Manen *et al.* 2005, 2006; Wapenaar & Fokkema 2006) and dissipative media (Snieder 2006), and this has been applied to obtain body wave estimates from controlled-source data (Bakulin & Calvert 2006) and in passive seismic data (Draganov *et al.* 2006; Forghani & Snieder 2010; Ruigrok *et al.* 2010). Mehta *et al.* (2007) demonstrate that when sources are not uniformly distributed around the receivers (e.g. if the medium of interest is illuminated from one side only), wavefield separation of the recorded wavefields into their upgoing and downgoing components can improve the quality of the virtual reflection response. This mitigates artifacts associated with the limited acquisition aperture typically used in practice, and constructs a virtual wavefield response deprived of downgoing reflections and multiples from the overburden above a subsurface (e.g. borehole) array of receivers and virtual sources.

In the non-ideal situation of limited arrays of sources and receivers, the correlation function is proportional to the Green's function from a source that is blurred in space and time. This blurring

is quantified by the so-called source point-spread function (PSF). An even more accurate estimate of the Green's function can be obtained by deconvolving the PSF from the correlation function. This is the essence of seismic interferometry by multidimensional deconvolution (MDD – Wapenaar *et al.* 2008b, 2011; Wapenaar & van der Neut 2010; Minato *et al.* 2011; van der Neut *et al.* 2011a; Vasconcelos & Rickett 2013; Nakata *et al.* 2014; van Dalen *et al.* 2014). The advantages of MDD over interferometry by cross-correlation are: (1) removal of the source signature, (2) improved radiation characteristics of the retrieved source and (3) relaxation of the assumptions of a closed surface of regularly sampled sources (e.g. one-sided illumination may be sufficient) and a lossless medium. On the other hand, the MDD approach also has limitations: (1) MDD requires a well-sampled array of receivers (it cannot be applied to a single-receiver configuration), (2) the measured wavefields must first be decomposed into up- and downgoing components for a complete cancellation of the effect of the overburden, requiring data acquisition using dual (i.e. pressure and particle velocity) receivers—while an estimate of the first arriving downgoing wave from single component receivers via time gating (van der Neut *et al.* 2011b) or single-trace deconvolution (Bellezza & Poletto 2014) can only compensate for the blurring effects and spread distortions, (3) the computational cost can be high due to the array operations involved and (4) the inverse problem that performs the deconvolution is usually ill-conditioned and hence must be regularized.

In this paper, we show that the preliminary step of separating measured wavefields into up- and downgoing components can be avoided. By using pressure and velocity data jointly in a system of MDD equations we invert simultaneously for pressure and velocity responses. To achieve this we use a two-way (full wavefield) representation, thus differing from conventional MDD that is based on a one-way (directional wavefield) representation. However, since twice the number of virtual responses are estimated using the same number of equations (this number depends on the number of available sources), the conditioning of two-way MDD is generally poorer than that of one-way MDD: while adding a regularization term on the solution norm is sometimes sufficient (as in one-way MDD), other filters (based, for example, on the directionality of the virtual responses that we want to retrieve) or sparsity constraints (van der Neut & Herrmann 2013) can be applied to better condition the inversion process when needed.

When used for borehole redatuming, two-way MDD improves the results of interferometry by cross-correlation by suppressing the effect of medium inhomogeneities in the overburden, and produces estimates of similar quality to those obtained by one-way MDD suggesting that the decomposition step is not required if pressure and velocity data are used jointly in the inversion. When two-way MDD is used for ocean-bottom multiple elimination, the virtual responses are still of good quality (clear improvements can be seen when compared to cross-correlation responses), although some interactions with the seabed are not entirely removed from the virtual gather unless directionality constraints are added to the inversion. Finally, representation theorems used for one- and two-way MDD are adapted to transform any type of available particle velocity receivers (e.g. normal or radial velocities) into their corresponding virtual dipole/gradient source. Thus we construct virtual data from virtual dipole or velocity source excitations, even though the original data are only excited by monopole sources. This is shown to be possible not only when dual data are acquired inside a borehole but also in marine streamer acquisition, provided that the information at near-offsets is carefully interpolated from available data (van der Neut *et al.* 2012).

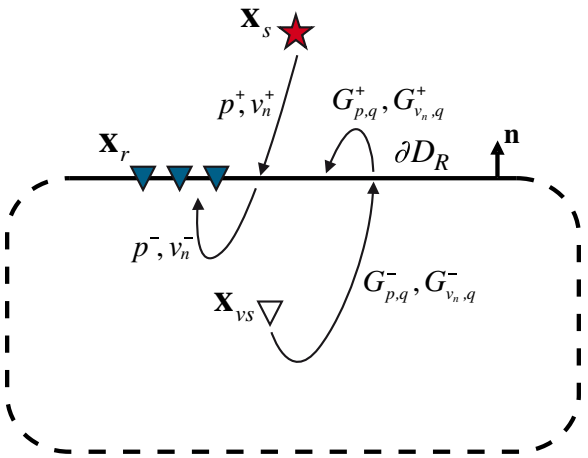

Figure 1. Acquisition geometry used in seismic interferometry by MDD. The red star denotes a source, blue triangles are receivers along the boundary ∂D_{R} and the white triangle refers to the receiver that seismic interferometry turns into a virtual source. The solid line corresponds to the portion of the surface ∂D_{R} where data are assumed to be available. Rays denote the decomposition of the wavefields in terms of waves that are either in- (down, +) or out- (up, −) going at the boundary.

ONE- AND TWO-WAY REPRESENTATION THEOREMS FOR SEISMIC INTERFEROMETRY

Recordings of waves propagating between $\mathbf{x}_s$ and $\mathbf{x}_{vs}$ in the geometrical configuration shown in Fig. 1 can be constructed by cross-convolution via the following two-way integral (Wapenaar *et al.* 2011)

$$p(\mathbf{x}_{vs}, \mathbf{x}_s, \omega) = \oint_{\partial D_R} p(\mathbf{x}_r, \mathbf{x}_s, \omega) G_{v_n,q}(\mathbf{x}_r, \mathbf{x}_{vs}, \omega) - v_n(\mathbf{x}_r, \mathbf{x}_s, \omega) G_{p,q}(\mathbf{x}_r, \mathbf{x}_{vs}, \omega)\, \mathrm{d}\mathbf{x}_r \qquad (1)$$

where for each angular frequency ω, p and v_n represent the pressure and normal particle velocity recorded at the receiver boundary ∂D_{R} from a monopole source at $\mathbf{x}_s$. $v_n = \mathbf{v}\cdot\mathbf{n}$ where $\mathbf{v}$ is the particle velocity vector and $\mathbf{n}$ is the outward pointing normal vector (Fig. 1). $G_{p,q}$ and $G_{v_n,q}$ denote the Green's functions from a monopole source (q) to pressure and normal velocity receivers, respectively, and in eq. (1) these Green's functions are from a virtual source located at $\mathbf{x}_{vs}$. It is important to remember that the fields p, v_n can represent a different wave state from $G_{p,q}$, $G_{v_n,q}$ and that p, v_n can be related to $G_{p,q}$, $G_{v_n,q}$ by reciprocity theorems inside ∂D_{R} where the medium is assumed to be the same for both states (Fokkema & van den Berg 1993). For example, $G_{p,q}$ and $G_{v_n,q}$ may belong to a state with different boundary conditions at ∂D_{R}, different sources, and/or different medium parameters outside of ∂D_{R}, compared to those that pertain to the waves in p and v_n.

In most practical situations, receivers are not available on a closed boundary, so the integration in eq. (1) is necessarily restricted to an open receiver boundary. However, as long as the source $\mathbf{x}_s$ is located outside of ∂D_{R}, it suffices to take the integral over an open receiver boundary such as the solid lines in Fig. 1 as Sommerfeld's radiation conditions (Sommerfeld 1954) may be assumed to apply on the half-sphere that would close the boundary, assuming that the half-sphere boundary radius is large (hence the contribution of the integral over that half-sphere vanishes). In the following we therefore replace the closed boundary integral by an open boundary integral.

The convolution-type integral in eq. (1), which is the basic expression for two-way seismic interferometry by cross-convolution, may be converted into its one-way (directional) counterpart as follows. We assume that all fields can be locally separated into in- (+) and outgoing (−) components at the boundary (see Appendix A for a brief review of wavefield separation and for a description of the associated requirements and limitations), such that $p = p^+ + p^-$ and $G_{v_n,q} = G^+_{v_n,q} + G^-_{v_n,q}$ (similarly for v_n and $G_{p,q}$) as illustrated in Fig. 1. Then eq. (1) is recast as

$$p = \int_{\partial D_R} \left(p^+ + p^-\right)\left(G^+_{v_n,q} + G^-_{v_n,q}\right) - \left(v^+_n + v^-_n\right)\left(G^+_{p,q} + G^-_{p,q}\right) \mathrm{d}\mathbf{x}_r. \quad (2)$$

Following the same reasoning used by Wapenaar & Berkhout (1989), Wapenaar & Fokkema (2006) and Vasconcelos *et al.* (2014), the two products between purely in-going terms at the stationary receiver locations (such receivers yield the dominant physical contributions to eq. 2) have opposite contributions that cancel, and this also happens for the products between the two outgoing terms. Consequently, these terms do not contribute to the convolution-type integral, such that eq. (2) can be reduced to

$$\begin{aligned} p(\mathbf{x}_{vs}, \mathbf{x}_s, \omega) = &\int_{\partial D_R} p^-(\mathbf{x}_r, \mathbf{x}_s, \omega) G^+_{v_n,q}(\mathbf{x}_r, \mathbf{x}_{vs}, \omega) \\ &+ p^+(\mathbf{x}_r, \mathbf{x}_s, \omega) G^-_{v_n,q}(\mathbf{x}_r, \mathbf{x}_{vs}, \omega)\, \mathrm{d}\mathbf{x}_r \\ &- \int_{\partial D_R} v^-_n(\mathbf{x}_r, \mathbf{x}_s, \omega) G^+_{p,q}(\mathbf{x}_r, \mathbf{x}_{vs}, \omega) \\ &+ v^+_n(\mathbf{x}_r, \mathbf{x}_s, \omega) G^-_{p,q}(\mathbf{x}_r, \mathbf{x}_{vs}, \omega)\, \mathrm{d}\mathbf{x}_r \\ = 2 &\int_{\partial D_R} p^-(\mathbf{x}_r, \mathbf{x}_s, \omega) G^+_{v_n,q}(\mathbf{x}_r, \mathbf{x}_{vs}, \omega) \\ &+ p^+(\mathbf{x}_r, \mathbf{x}_s, \omega) G^-_{v_n,q}(\mathbf{x}_r, \mathbf{x}_{vs}, \omega)\, \mathrm{d}\mathbf{x}_r \end{aligned} \quad (3)$$

where we have also used the fact that terms $p^- G^+_{v_n,q}$ and $-v^-_n G^+_{p,q}$ (as well as $p^+ G^-_{v_n,q}$ and $-v^+_n G^-_{p,q}$) give equal contributions to the integral to further reduce the number of terms involved in the integral relation 3.

In addition, we are free to choose convenient boundary conditions at ∂D_R and medium parameters outside ∂D_R, for G. We choose a specific type of Green's function that has only the outward propagating term—i.e. $G_{v_n,q} = G^-_{v_n,q}$, that is $G^+_{v_n,q} = 0$. Effectively then ∂D_R acts as an absorbing boundary for $G_{v_n,q}$, or equivalently the medium is homogenous outside of ∂D_R as shown in Fig. 2 (Wapenaar *et al.* 2011). Eq. (3) then simplifies to

$$p(\mathbf{x}_{vs}, \mathbf{x}_s, \omega) = 2\int_{\partial D_R} p^+(\mathbf{x}_r, \mathbf{x}_s, \omega) G^-_{v_n,q}(\mathbf{x}_r, \mathbf{x}_{vs}, \omega)\, \mathrm{d}\mathbf{x}_r. \quad (4)$$

Eqs (1) and (4) are the respective starting points for two- and one-way interferometry by deconvolution. If terms $G_{v_n,q}$ and $G_{p,q}$ (or alternatively $G^-_{v_n,q}$) inside the integrals are the unknown quantities to be estimated, these equations need to be solved by MDD. For applications of MDD where $\mathbf{x}_{vs}$ is a receiver on ∂D_R, it is often useful to consider only the outward propagating part of the field at $\mathbf{x}_{vs}$ by applying decomposition also on the left hand side of eq. (4) [the outgoing part is $p^-(\mathbf{x}_{vs}, \mathbf{x}_s, \omega)$]. Whether the input on the left of equation 4 is the full pressure field p or only the upgoing part of the pressure field p^- controls whether or not the estimated Green's function from $\mathbf{x}_{vs}$ to $\mathbf{x}_r$ contains the direct wave or not (see Amundsen 2001).

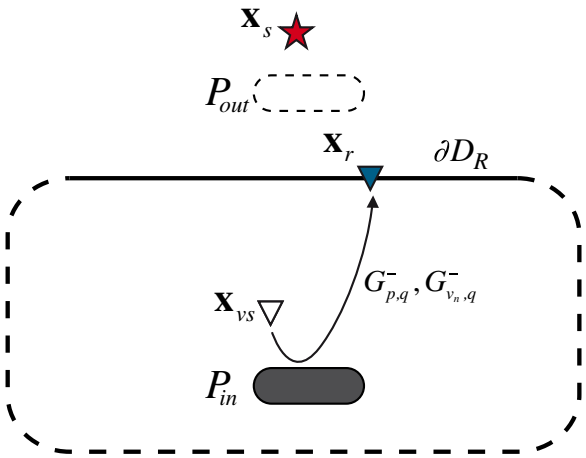

Figure 2. Cartoon denoting the choice of the Green's function wave state in the one-way representation (eq. 5). Although both perturbations outside (P_{out} – white dashed region) and inside (P_{in} – grey region) the boundary ∂D_{R} belong to the wave state of the recorded data, the medium is assumed to be homogeneous outside of the boundary ∂D_{R} in the Green's function wave state, so only the perturbation inside surface ∂D_{R} is included in the Green's function state and hence in the solutions obtained. Keys as in Fig. 1.

ONE- AND TWO-WAY INTERFEROMETRY BY MDD

Interferometry by MDD essentially consists of inverting eqs (1) or (4) for the unknown Green's functions. If there was a single source (and so a single equation), the inverse problem would be ill-posed. However, these equations hold for each source position $\mathbf{x}_s$ outside of ∂D_{R}. Solving the ensemble of equations for any G is a better posed problem. Nevertheless, the existence of the relevant inverse operator is not guaranteed (indeed it seldom exists in practice) and its conditioning depends on many factors such as the number of available sources, the source array aperture, and the source bandwidth.

One-way MDD

We first consider MDD using the one-way representation. For the inversion of eq. (4) we first define $G^-_{ow} = 2G^-_{v_n,q}$, discretize the integration along the receivers to a summation, and write the equation in matrix form for each angular frequency separately

$$\mathbf{p} = \mathbf{p}^+ \mathbf{G}^-_{\mathbf{ow}}, \quad (5)$$

where $\mathbf{p}^+$ is a data matrix with rows and columns corresponding to source locations $\mathbf{x}_s$ and receiver locations $\mathbf{x}_r$, respectively. Similarly $\mathbf{p}$ is a matrix with rows and columns corresponding to source locations $\mathbf{x}_s$ and virtual source locations $\mathbf{x}_{vs}$. Finally $\mathbf{G}^-_{\mathbf{ow}}$ is a matrix with rows and columns corresponding to receiver locations $\mathbf{x}_r$ and virtual source locations $\mathbf{x}_{vs}$.

We then define our objective: to obtain a least-squares estimate of the unknown Green's functions $\mathbf{G}^-_{\mathbf{ow}}$ by minimizing the misfit

$$J^-_{ow} = \left\| \mathbf{p} - \mathbf{p}^+ \mathbf{G}^-_{\mathbf{ow}} \right\|_2, \quad (6)$$

where subscript 2 denotes the *l2*-norm. Via some algebra (Menke 1989), the solution of eq. (6) can be written as the normal equation

$$\mathbf{C}^-_{\mathbf{ow}} = \mathbf{\Gamma}^-_{\mathbf{ow}} \mathbf{G}^-_{\mathbf{ow}} \Leftrightarrow \mathbf{G}^-_{\mathbf{ow}} = \left(\mathbf{\Gamma}^-_{\mathbf{ow}}\right)^{-1} \mathbf{C}^-_{\mathbf{ow}}, \quad (7)$$

where $\mathbf{\Gamma}^-_{\mathbf{ow}} = \left(\mathbf{p}^+\right)^H \mathbf{p}^+$ and $\mathbf{C}^-_{\mathbf{ow}} = \left(\mathbf{p}^+\right)^H \mathbf{p}$ with H denoting the conjugate transpose matrix. After Wapenaar *et al.* (2011) and van

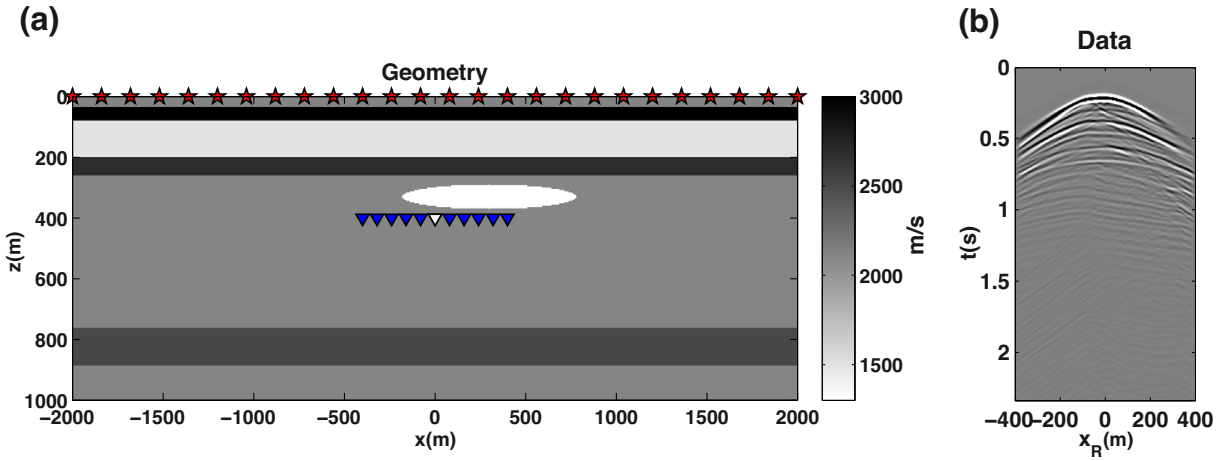

Figure 3. (a) Configuration for borehole redatuming. Sources (red stars) are situated at the earth's surface, while receivers (blue triangles) and the virtual source (white triangle) are in a well below a 'complex' overburden. (b) Recorded pressure data from source at $x_s = 0$ m.

der Neut *et al.* (2011a), $\mathbf{\Gamma}^-_{\mathbf{ow}}$ is hereafter referred to as a wavefield PSF, while the matrix $\mathbf{C}^-_{\mathbf{ow}}$ is the cross-correlation function. Eq. (7) states that the correlation function $\mathbf{C}^-_{\mathbf{ow}}$ is proportional to the sought Green's function $\mathbf{G}^-_{\mathbf{ow}}$, smeared in space and time by $\mathbf{\Gamma}^-_{\mathbf{ow}}$.

Exact minimization of J^-_{ow} generally results in an unstable solution that is not desired. Numerical instability can be prevented by introducing an additional constraint on the solution norm (commonly referred to as regularization):

$$J^-_{ow} = \left\| \mathbf{p} - \mathbf{p}^+ \mathbf{G}^-_{\mathbf{ow}} \right\|_2 + \lambda_G^2 \left\| \mathbf{G}^-_{\mathbf{ow}} \right\|_2 \tag{8}$$

and the solution of eq. (8) is then

$$\mathbf{G}^-_{\mathbf{ow}} = \left(\mathbf{\Gamma}^-_{\mathbf{ow}} + \lambda_G^2 \mathbf{I} \right)^{-1} \mathbf{C}^-_{\mathbf{ow}} = \left(\mathbf{\Gamma}^-_{\mathbf{ow}} \right)^{\dagger} \mathbf{C}^-_{\mathbf{ow}}, \tag{9}$$

where λ_G controls the balance between minimizing the data residual (low λ_G) and the solution norm (high λ_G). Here $\dagger$ is used to identify the regularized inverse and $\left(\mathbf{\Gamma}^-_{\mathbf{ow}}\right)^{\dagger}$ is the regularized inverse of the one-way PSF.

Two-way MDD

The two-way representation in eq. (1) is now converted into matrix equations suitable for inversion. Arranging the fields $p(\mathbf{x}_r, \mathbf{x}_s, \omega)$ and $v_n(\mathbf{x}_r, \mathbf{x}_s, \omega)$ into matrices $\bar{\mathbf{p}}$ and $\bar{\mathbf{v}}$ (a bar is added to emphasize that these are full data recorded by receivers $\mathbf{x}_r$ as opposed to virtual sources $\mathbf{x}_{vs}$ as in absence of the bar), and the Green's functions $G_{p,q}(\mathbf{x}_r, \mathbf{x}_{vs}, \omega)$ and $G_{v_n,q}(\mathbf{x}_r, \mathbf{x}_{vs}, \omega)$ into matrices $\mathbf{G}_{\mathbf{p}}$ and $\mathbf{G}_{\mathbf{v}}$ similarly to above, we can write

$$\mathbf{p} = \begin{bmatrix} \bar{\mathbf{p}} & -\bar{\mathbf{v}} \end{bmatrix} \begin{bmatrix} \mathbf{G}_{\mathbf{v}} \\ \mathbf{G}_{\mathbf{p}} \end{bmatrix} \Leftrightarrow \mathbf{p} = \mathbf{d}\mathbf{G}_{\mathbf{tw}}, \tag{10}$$

where $\mathbf{d}$ is the first matrix composed of the concatenation of pressure and (negative) velocity data, and $\mathbf{G}_{\mathbf{tw}}$ is the second matrix composed of the concatenation of velocity and pressure of the unknown Green's functions. The least squares solution is again obtained by minimizing the misfit

$$J_{tw} = \|\mathbf{p} - \mathbf{d}\mathbf{G}_{\mathbf{tw}}\|_2 + \lambda_G^2 \|\mathbf{G}_{\mathbf{tw}}\|_2 \tag{11}$$

and the solution is

$$\mathbf{G}_{\mathbf{tw}} = \left(\mathbf{\Gamma}_{\mathbf{tw}} + \lambda_G^2 \mathbf{I} \right)^{-1} \mathbf{C}_{\mathbf{tw}} = \left(\mathbf{\Gamma}_{\mathbf{tw}} \right)^{\dagger} \mathbf{C}_{\mathbf{tw}}, \tag{12}$$

where the PSF and cross-correlation matrices are block matrices composed of different combinations of pressure and velocity data:

$$\begin{aligned} \mathbf{\Gamma}_{\mathbf{tw}} &= (\mathbf{d})^H \mathbf{d} = \begin{bmatrix} (\bar{\mathbf{p}})^H \bar{\mathbf{p}} & -(\bar{\mathbf{p}})^H \bar{\mathbf{v}} \\ -(\bar{\mathbf{v}})^H \bar{\mathbf{p}} & (\bar{\mathbf{v}})^H \bar{\mathbf{v}} \end{bmatrix}, \\ \mathbf{C}_{\mathbf{tw}} &= (\mathbf{d})^H \mathbf{p} = \begin{bmatrix} (\bar{\mathbf{p}})^H \mathbf{p} \\ -(\bar{\mathbf{v}})^H \mathbf{p} \end{bmatrix} \end{aligned} \tag{13}$$

and $\left(\mathbf{\Gamma}_{\mathbf{tw}}\right)^{\dagger}$ is the regularized inverse of the two-way PSF.

Directional constraints on two-way MDD

In order to define a wave state uniquely, medium parameters, boundary conditions and sources type need to be selected. We know that the convolution-type representation used as a starting point for seismic interferometry by MDD allows for an arbitrary choice of the Green's function wave state with possibly different boundary conditions at ∂D_{R} and medium parameters outside of ∂D_{R} from those of the data. In the one-way representation, Wapenaar *et al.* (2011) choose the medium to be homogeneous outside of boundary ∂D_{R} (i.e. $G^+_{v_n,q} = 0$). This implies that the sought Green's function is uniquely defined. However, this particular condition cannot be used directly for the two-way representation because full fields are used in eq. (1) rather than up- and downgoing separated fields: the solution obtained by solving eq. (11) via MDD thus mainly depends on the minimization criterion and regularization applied. Additional linear constraints can be applied to drive the inversion towards a particular desired Green's function solution.

For comparison with existing methods, here we show how we can estimate the solution of one-way MDD (in case that is what is desired) by implicitly ensuring that the downgoing Green's function components $G^+_{v_n,q}$ and/or $G^+_{p,q}$ go to zero. In order to do so, we first need to recall the decomposition operators in the frequency-wavenumber domain that, when applied to pressure and velocity time and space Fourier transformed fields, identify their downgoing components:

$$\mathbf{D}^+_{\mathbf{p}} = \frac{1}{2} \begin{bmatrix} \xi(k_{x,r})\mathbf{I} & \mathbf{I} \end{bmatrix}, \quad \mathbf{D}^+_{\mathbf{v}} = \frac{1}{2} \begin{bmatrix} \mathbf{I} & 1/\xi(k_{x,r})\mathbf{I} \end{bmatrix} \tag{14}$$

where ξ is the so-called obliquity factor and $k_{x,r}$ is the horizontal wavenumber at the receiver array (see Appendix A for their derivation). To be able to apply directionality constraints to the two-way representation in either eq. (1) or its discretized version in eq. (10), we first transform these equations from the frequency–space to the frequency–wavenumber domain by assuming that an array of receivers $\mathbf{x}_r$ is available along a horizontal line (in 2-D) or plane (in 3-D) and make use of Parceval's identity (Amundsen 2001) resulting in

$$p(\mathbf{x}_{vs}, \mathbf{x}_s, \omega) = \int_{-\infty}^{+\infty} p(-k_{x,r}, \mathbf{x}_s, \omega) G_{v_n,q}(k_{x,r}, \mathbf{x}_{vs}, \omega) - v_n(-k_{x,r}, \mathbf{x}_s, \omega) G_{p,q}(k_{x,r}, \mathbf{x}_{vs}, \omega)\, \mathrm{d}k_{x,r}. \quad (15)$$

Note that the recorded data on the left-hand side of eq. (15) remains in the frequency-space domain since we only need to transform across the receiver array. After discretizing eq. (15) in the same way as for eq. (1), the directionality constraints can be added to the least-squares objective function:

$$J_{tw}^{-} = J_{tw} + \lambda_{D_p}^2 \left\| \mathbf{D}_{\mathbf{p}}^{+} \mathbf{G}_{\mathbf{tw}} \right\|_2 + \lambda_{D_v}^2 \left\| \mathbf{D}_{\mathbf{v}}^{+} \mathbf{G}_{\mathbf{tw}} \right\|_2. \quad (16)$$

Parameters λ_{D_p} and λ_{D_v} control the extent to which we wish the solution to contain less downgoing than upgoing energy (larger values of λ_{D_p} and λ_{D_v} result in less downgoing energy). The solution of the minimization problem in eq. (16) is

$$\mathbf{G}_{\mathbf{tw}} = \left(\mathbf{\Gamma}_{\mathbf{tw}} + \lambda_{D_p}^2 \left(\mathbf{D}_{\mathbf{p}}^{+} \right)^H \mathbf{D}_{\mathbf{p}}^{+} + \lambda_{D_v}^2 \left(\mathbf{D}_{\mathbf{v}}^{+} \right)^H \mathbf{D}_{\mathbf{v}}^{+} + \lambda_G^2 \mathbf{I} \right)^{-1} \mathbf{C}_{\mathbf{tw}} = \left(\mathbf{\Gamma}_{\mathbf{tw}}^{-} \right)^{\dagger} \mathbf{C}_{\mathbf{tw}}. \quad (17)$$

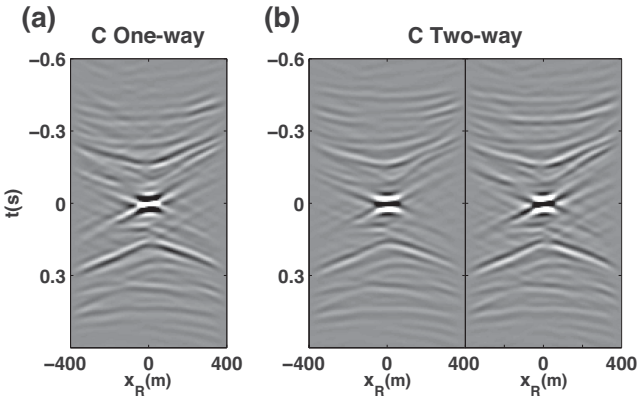

Figure 4. (a) Interferometry by cross-correlation of decomposed wavefields (i.e. one-way representation), compared with (b) cross-correlation of full wavefields (i.e. two-way representation) for the configuration in Fig. 3a. In the two-way cross-correlation, each side of (b) represents a block in eq. (13). Left is $(\bar{\mathbf{p}})^H \mathbf{p}$ and right is $-(\bar{\mathbf{v}})^H \mathbf{p}$.

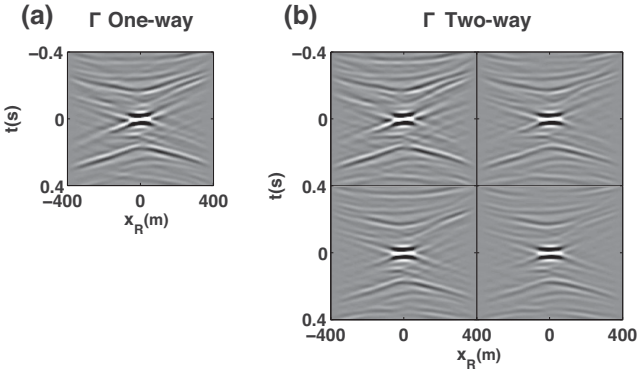

Figure 5. PSFs of (a) one-way and (b) two-way MDD for the configuration in Fig. 3a. In two-way MDD, the PSF is a block matrix and each quadrant in (b) represents a block in eq. (13). Top left is $(\bar{\mathbf{p}})^H \bar{\mathbf{p}}$, top right is $-(\bar{\mathbf{p}})^H \bar{\mathbf{v}}$, bottom left is $-(\bar{\mathbf{v}})^H \bar{\mathbf{p}}$, and bottom right is $(\bar{\mathbf{v}})^H \bar{\mathbf{v}}$.

Virtual dipole sources with one- and two-way MDD

Particle velocity measurements are generally required by algorithms for wavefield decomposition, both as a pre-processing step for one-way MDD as well as by two-way MDD to directly estimate virtual recordings. These measurements (or the up- and downgoing fields obtained by combining them with pressure data) are taken into account at the receiver locations $\mathbf{x}_r$ in representation theorems 1 and 4, while only pressure data are used at the virtual source location $\mathbf{x}_{vs}$. However, if we multiply each side of eq. (1) by the operator that transforms pressure fields into particle velocity fields (i.e. $-(j\omega\rho)^{-1}\partial_i$ to obtain particle velocity in coordinate direction i) at the virtual source location, we can create a modified representation theorem that allows us to estimate pressure and normal particle velocity Green's functions from dipolar (spatial derivative) sources (f_i) at the virtual source location, provided that we have appropriate velocity (and/or pressure array) sensors at the virtual source locations:

$$v_i(\mathbf{x}_{vs}, \mathbf{x}_s, \omega) = \oint_{\partial D_R} p(\mathbf{x}_r, \mathbf{x}_s, \omega) G_{v_n,f_i}(\mathbf{x}_r, \mathbf{x}_{vs}, \omega) - v_n(\mathbf{x}_r, \mathbf{x}_s, \omega) G_{p,f_i}(\mathbf{x}_r, \mathbf{x}_{vs}, \omega)\, \mathrm{d}\mathbf{x}_r \quad (18)$$

with $i = x,z$ (or any other direction obtained by combining the available velocity measurements). Similarly the one-way representation in eq. (4) can be written as

$$v_i(\mathbf{x}_{vs}, \mathbf{x}_s, \omega) = 2 \int_{\partial D_R} p^{+}(\mathbf{x}_r, \mathbf{x}_s, \omega) G_{v_n,f_i}^{-}(\mathbf{x}_r, \mathbf{x}_{vs}, \omega)\, \mathrm{d}\mathbf{x}_r. \quad (19)$$

By solving eqs (18) or (19) via MDD, pressure and normal velocity responses from virtual dipole sources can be estimated for

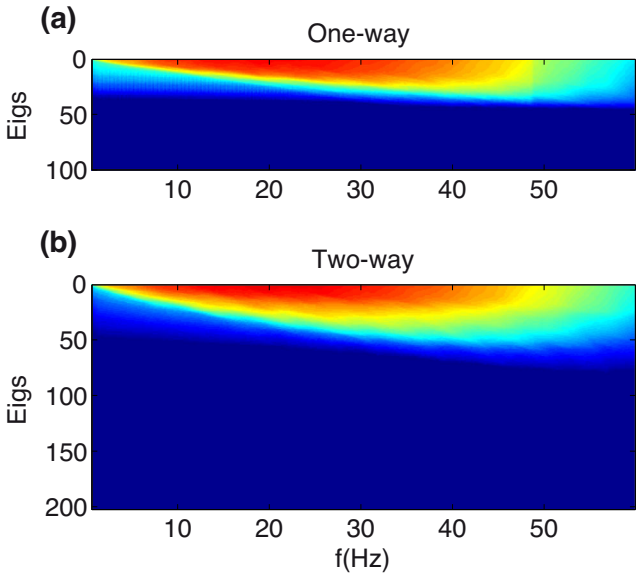

Figure 6. Singular values at each frequency for PSF matrices: for the configuration in Fig. 3a. (a) one-way MDD (matrix $\mathbf{\Gamma}_{ow}^{-}$), and (b) two-way MDD (matrix $\mathbf{\Gamma}_{tw}$). Singular values are coloured using a logarithmic scale and re-sorted in ascending order where red indicates high values and blue low values.

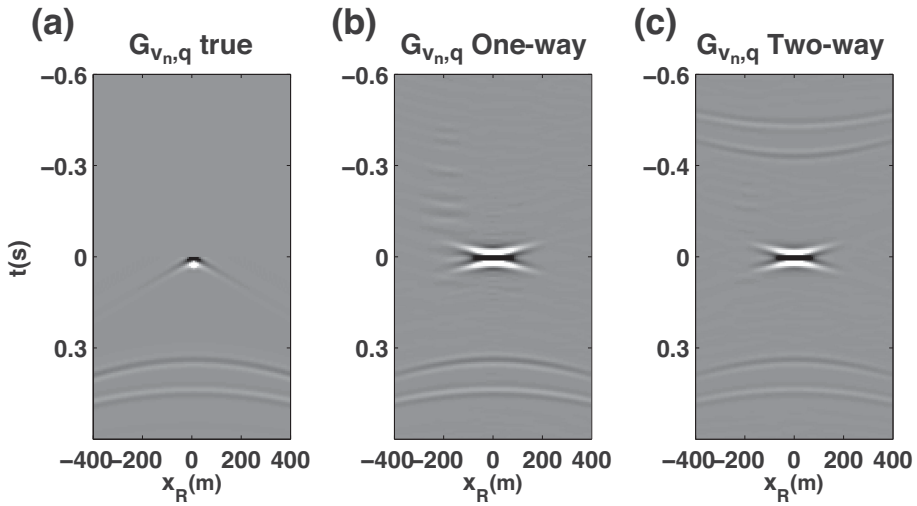

Figure 7. Velocity Green's function from a virtual monopole (pressure) source for the configuration in Fig. 3a. (a) Modelled response, and solutions from (b) one-way MDD and (c) two-way MDD.

pressure and normal velocity recordings at virtual locations, even if only monopolar sources are available in the physical experiment.

EXAMPLES

We now use synthetic examples to explore the relative effectiveness of correlational, and one- and two-way MDD based interferometry for Green's function estimation. There are important differences between the data that can be acquired in borehole, ocean bottom and marine seismics so we investigate each in turn.

Borehole redatuming

In our first example the seismic wavefield generated by sources at the Earth's surface is measured by receivers in a horizontal borehole below a complex overburden. Seismic interferometry redatums sources into virtual sources in the borehole (Bakulin & Calvert 2006) and MDD removes the effects of medium inhomogeneities between sources and receivers (Wapenaar & van der Neut 2010). The complex overburden is here composed of fine layers and a gas cloud (white ellipse) that acts as an acoustic lens, while a target such as a hydrocarbon reservoir is located around 800m depth (Fig. 3a).

Data (Fig. 3b) are generated from an array of 251 sources with spacing $\Delta x_s = 16m$ firing into 101 dual receivers spaced at $\Delta x_r = 8m$ using a finite-difference code which models the full set of acoustic first-order partial differential equations for pressure and particle velocity (Fokkema & van den Berg 1993) in a staggered-grid scheme. The source excitation function is a zero-phase Ricker wavelet with a 20 Hz peak frequency, and absorbing boundaries are placed on all sides of the model. To perform wavefield separation of the recorded data in the frequency-wavenumber domain (see Appendix A for the mathematical derivation), we assume that the medium properties at the receiver level are known (here they are $c = 2100$ m s^{-1} and $\rho = 1000$ kg m^{-3}).

Fig. 4 shows the correlation functions for one- and two-way interferometry. The response of the reservoir is not clearly visible in the correlation functions (compare with Fig. 7a) because strong coherent events arising from cross-talk between upgoing and downgoing events populate the gathers. The effect of these events can similarly be observed in the PSFs in Fig. 5, which deviate from band-limited delta functions, and which need to be inverted and deconvolved by MDD: according to eqs (7) and (12), the correlation functions in Fig. 4 can be seen as the desired response convolved in space and time with the PSFs in Fig. 5. Note that since in the one-way case we auto-correlate the downgoing field to construct the PSF, spurious events are fewer compared to those in the two-way case where the full field is used. This is natural because significantly more information is implicit (assumed) in the one-way equations, specifically the wavefield decomposition into up- and downgoing fields.

Generally the more the PSF deviates from a band-limited delta function, the more the MDD becomes ill-posed and extra care has to be taken in the inversion. This can be observed in the eigenvalues of the PSFs for each frequency (Fig. 6): although two-way MDD has doubled the dimensions of the PSF, almost half of its most significant singular values are very similar to those of one-way MDD (Fig. 6a), while the remaining half are close to zero (Fig. 6b) making the problem severely ill-posed.

The benefit of deconvolving the PSF is illustrated in Fig. 7: when its effect is removed from the correlation functions, the

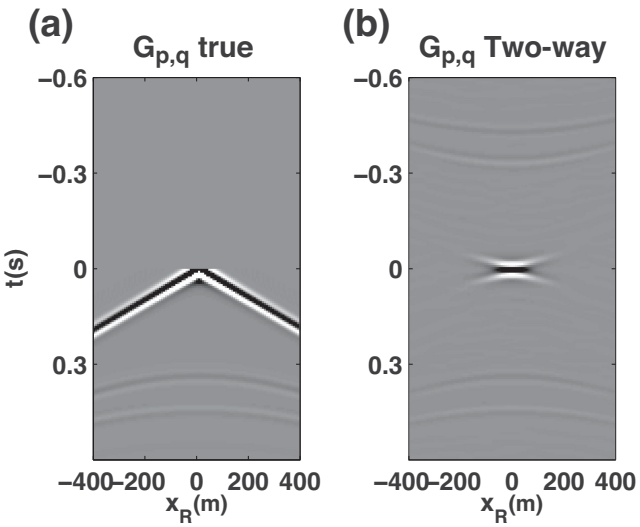

Figure 8. Pressure Green's function from a virtual monopole source for the configuration in Fig. 3a. (a) Modelled response and solution from (b) two-way MDD.

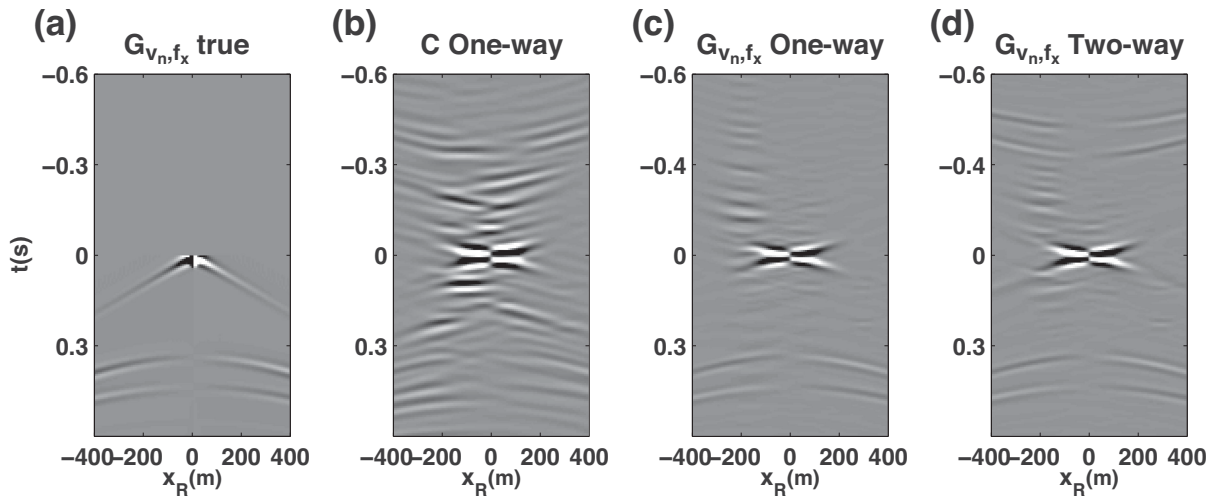

Figure 9. Velocity Green's function from a virtual horizontal dipole source for the configuration in Fig. 3a. (a) Modelled response, (b) result of interferometry by cross-correlation, and solutions from (c) one-way MDD and (d) two-way MDD.

match between the directly modelled response from the reservoir (Fig. 7a) and that from one-way MDD (Fig. 7b) and two-way MDD by means of eq. (12) (Fig. 7c) is much improved. The retrieved responses are in fact free of multiple scattering caused by the geological layers and gas cloud in the overburden. Note also that, since the recorded pressure and normal velocity fields are used directly in the inversion, two-way MDD does not require any (accurate) estimate of medium properties along the receiver array to be successful.

Interestingly, the Green's functions retrieved by two-way MDD by means of eq. (12) shows symmetry with respect to the time axis, even though we would expect energy only in the causal part of the virtual field as stated in eqs (1) and (10). Mathematically speaking, events in the anticausal part of the solution of two-way MDD are the direct consequence of choosing a regularization term that favours the minimum norm solution [i.e. $(\Gamma_{\rm tw})^{\dagger} = (\Gamma_{\rm tw} + \lambda \mathrm{I})^{-1}$]: by making the Green's function real and symmetric in time, events in the anticausal part make the solution also real and symmetric in frequency, thus cancelling its imaginary component and minimizing its total energy (and hence also its norm). Moreover, as shown in Appendix B, there is also a physical reason for the retrieval of the anticausal part of the Green's function. $G^{*}_{v_n,q}$ and $G^{*}_{p,q}$ are in fact solutions of the correlation-type representation theorem (eq. B1) that involves the same recorded data p and v_n of the convolution-type representation theorem in eq. (1). However, it is important to note that the contribution of the half-sphere closing the boundary $\partial D_{\rm R}$ in Fig. 1 cannot be neglected since radiation conditions cannot be applied to the correlation-type representation (Wapenaar & Fokkema 2006). Therefore we expect the anticausal estimate to be less trustworthy than the causal one in scenarios where receivers are not available on a closed boundary. We thus suggest to use the causal response as the estimate of the Green's function for two-way MDD. Additionally, seismic interferometry by means of two-way representations also recovers an estimate of the pressure Green's function as shown in Fig. 8. Note that in this case the anticausal part of the estimated Green's functions again contains arrivals from the reservoir but the polarity is reversed compared to the causal component (as expected – see Appendix B).

We then applied seismic interferometry by MDD to monopole (pressure and particle velocity) data to construct virtual dipole sources from particle velocity receivers by inverting the representation theorems in eqs (18) and (19). In particular, by using the horizontal component of the recorded field ($i = x$) in the left-hand side of these equations, we reconstruct Green's functions from a virtual horizontal dipole source to velocity (Fig. 9) and pressure (Fig. 10) receivers. The improvement arising by deconvolving the PSF from the one-way cross-correlation function [$\mathbf{C}^{-}_{\rm ow} = \left(\mathbf{p}^{+}\right)^{H}\ \mathbf{v}_{\rm x}$ – Fig. 9b] is shown in Figs 9(c), (d) and 10(b). When one-way MDD is used, cross-talk events that overlap the response of the reservoir in the cross-correlation gather are properly mitigated, leaving only the events of interest with their characteristic dipolar radiation pattern in the deconvolved response (Fig. 9c). Two-way MDD is also proven to produce equally good estimates of the normal velocity Green's function (Fig. 9d) together with the pressure Green's function (Fig. 10b) using full (rather than decomposed) pressure and velocity fields. We refer to Appendix B for a discussion on the polarity of causal and anticausal solutions.

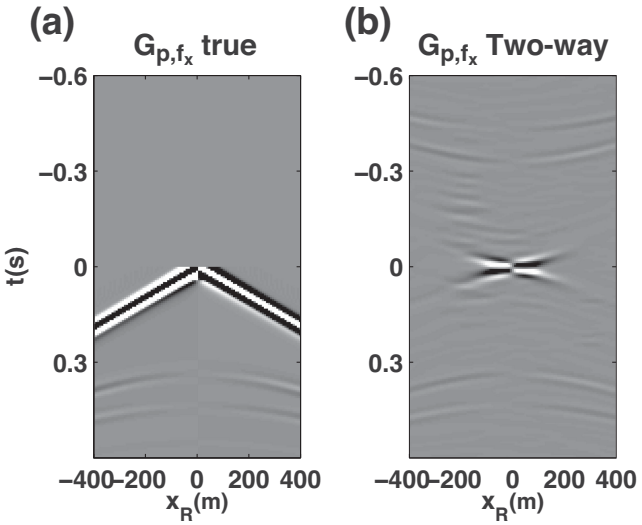

Figure 10. Pressure Green's function from a virtual horizontal dipole source for the configuration in Fig. 3a. (a) Modelled response and (b) solution from two-way MDD.

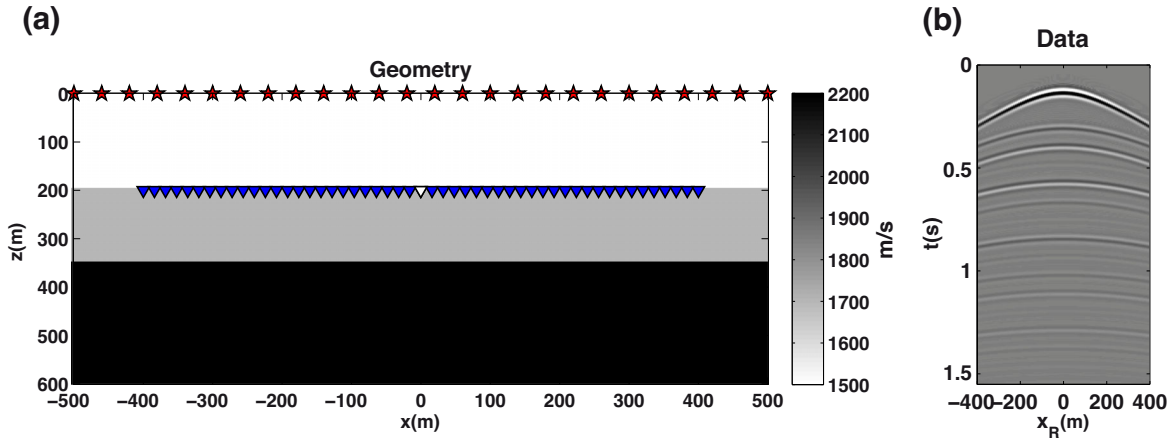

Figure 11. (a) Configuration for ocean-bottom multiple elimination. Sources (red stars) are situated just below the top surface, while receivers (blue triangles) and virtual source (white triangle) are at the ocean bottom. (b) Recorded pressure data from source at $x_S = 0$ m.

Ocean-bottom multiple elimination

As discussed extensively in van der Neut *et al.* (2011a) and Wapenaar *et al.* (2011), interferometry by MDD is akin to multiple elimination when applied to ocean-bottom data (Ziolkowski *et al.* 1999; Amundsen 2001). Here we apply one-way and two-way interferometry by MDD to synthetic acoustic data generated using an array of 126 sources with spacing $\Delta x_s = 8m$ deployed just below the water surface and 101 dual receivers (recording acoustic pressure and normal particle velocity) spaced at $\Delta x_r = 8m$ at the ocean bottom (Fig. 11a). Our objective is to synthetize the virtual response of the half-space below ∂D_R, without any multiple reflections related to the ocean bottom and the water surface that affect the recorded data (Fig. 11b), and to test whether this is also possible using two-way MDD.

We use a model composed of three horizontal layers: the first layer is water ($v = 1500$ m s^{-1}), while the second and third layers have velocities 1700 and 2200 m s^{-1}, respectively (Fig. 11). Data are generated using a zero-phase Ricker wavelet with 20 Hz peak frequency, a free-surface at the top of the model and absorbing boundaries on all other sides of the model. Wavefield decomposition is applied to the dual recordings at the ocean bottom using the medium parameters of the first layer below the ocean bottom to obtain the downgoing pressure field $p^+(\mathbf{x}_r, \mathbf{x}_s, t)$ just below the ocean bottom (Amundsen & Reitan 1995; Schalkwijk *et al.* 2003).

The correlation function (Fig. 12a) and PSF (Fig. 13a) are then computed for the one-way model by eq. (7) and compared to those of the two-way model in eq. (13) (Figs 12b and 13b). The match of both correlation functions with the response of the interface below the receiver array (Fig. 14a) is reasonably good, however the correlation gathers also contain many spurious multiple reflections due to the crosstalk between upgoing and downgoing events in the data. Moreover, apart from band-limited delta functions around $x_r = 0, t = 0$, the PSFs also contain multiple reflections.

The results of the MDD procedure are shown in Fig. 14: the effect of spurious multiples in Fig. 12 have been mitigated by either one- or two-way MDD and an estimate of the velocity Green's function (for a virtual monopole source $\mathbf{x}_{vs}$ fixed at the central receiver—the white triangle in Fig. 11) is obtained. We notice however that when the two-way representation theorem is solved via MDD without directional constraints as in eq. (12) (Fig. 14c), the retrieved Green's function not only shows symmetry with respect to the time axis as in the previous example, but weak residual energy of multiple events from the seabed around ± 0.4 s also remains in the MDD estimate. This indicates that the basic two-way MDD is less successful than one-way MDD in removing the effect of the overburden, in this seabed case.

As in the previous example, the difference in the solution of two-way MDD compared to that of one-way MDD (Fig. 14b) is

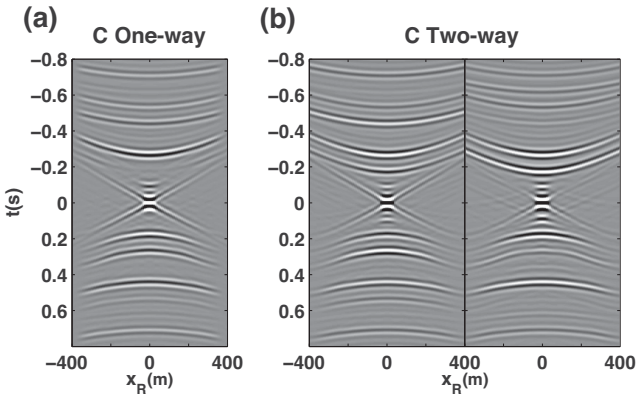

Figure 12. (a) Interferometry by cross-correlation of (a) decomposed wavefields and (b) full wavefields for the configuration in Fig. 11a. In (b) the left-hand side is $(\bar{\mathbf{p}})^H\,\mathbf{p}$ and the right-hand side is $-(\bar{\mathbf{v}})^H\,\mathbf{p}$.

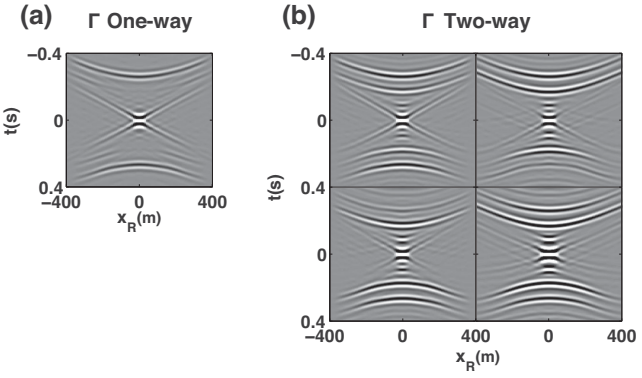

Figure 13. PSF of (a) one-way interferometry by MDD and (b) two-way interferometry by MDD for the configuration in Fig. 11a. In two-way MDD, the PSF is a block matrix and each quadrant in (b) represents a block in eq. (13). Top left is $(\bar{\mathbf{p}})^H\,\bar{\mathbf{p}}$, top right is $-(\bar{\mathbf{p}})^H\,\bar{\mathbf{v}}$, bottom left is $-(\bar{\mathbf{v}})^H\,\bar{\mathbf{p}}$ and bottom right is $(\bar{\mathbf{v}})^H\,\bar{\mathbf{v}}$.

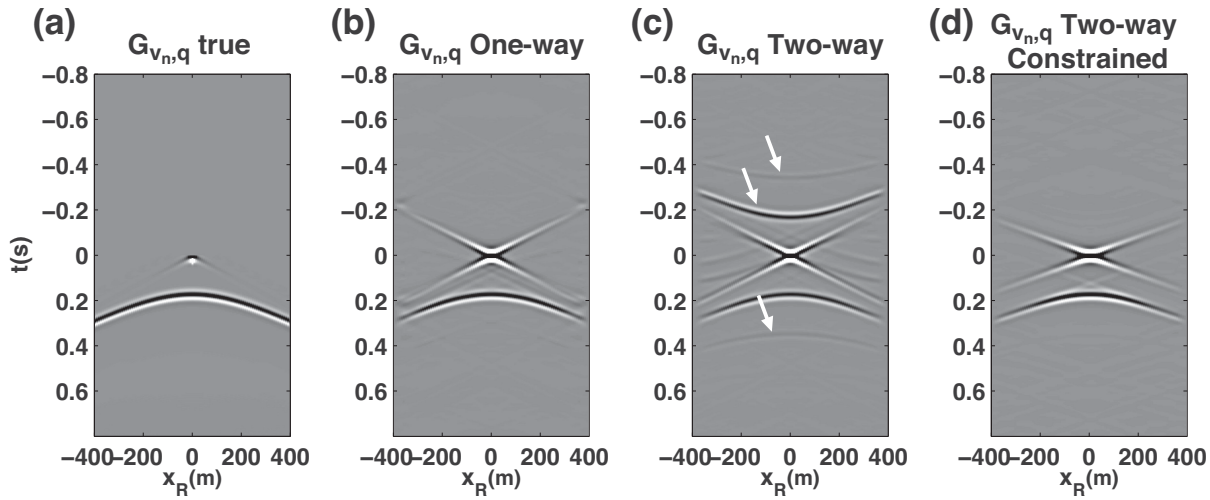

Figure 14. Velocity Green's function from a virtual monopole source for the configuration in Fig. 11a. (a) Modelled response, and solutions from (b) one-way MDD, (c) two-way MDD and (d) two-way directionally constrained MDD. White arrows indicate events that are reconstructed by two-way MDD and suppressed using a directional constraint in two-way constrained MDD.

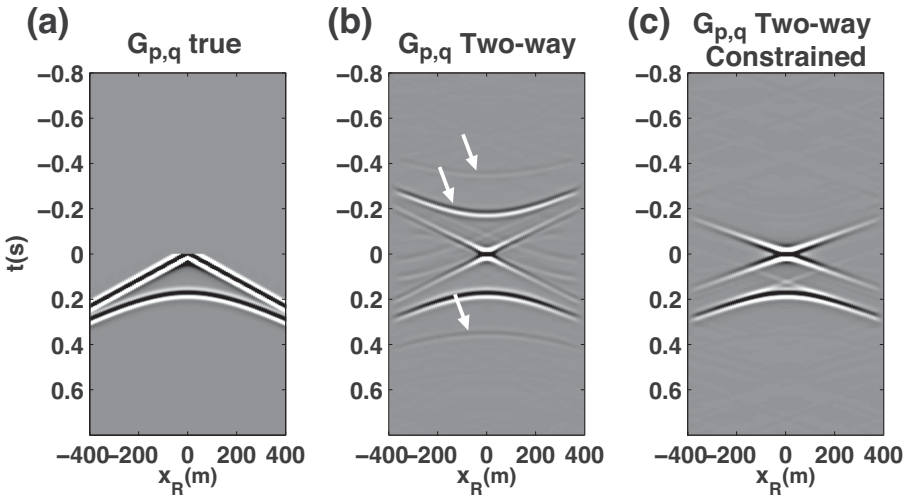

Figure 15. Pressure Green's function from a virtual monopole source for the configuration in Fig. 11a. (a) Modelled response, and solutions from (b) two-way MDD and (c) two-way directionally-constrained MDD.

a consequence of the fact that any pair of Green's functions $G_{p,q}$ and $G_{v_n,q}$ that fit the recorded data, and which belong to a state with the same medium parameters as the recorded data p and v_n inside ∂D_R, but possibly different boundary conditions at ∂D_R and/or different medium parameters outside ∂D_R, are a valid choice of Green's functions for the representation theorem in eqs (1) and (2). By adding boundary constraints on the directionality of the pressure and velocity Green's functions to the two-way representation (eq. 11) as shown in eq. (16), we define the particular Green's function that we wish to estimate and the solution of two-way constrained MDD (Fig. 14d) becomes very similar to that retrieved by one-way MDD (Fig. 14b). We have noted that these directionality constraints are particularly beneficial in the case of receivers sitting on a discontinuity (e.g. the seabed) that generates prominent multiples in the data. In fact, by using the medium parameters of the layer below the ocean bottom in the directionality constraints (as well as in wavefield decomposition applied before one-way MDD), we have enforced the receiver line to be below the seabed, such that its effect is suppressed by MDD. This was not possible in unconstrainted two-way MDD because the recordings were directly used in the inversion process. Additionally, seismic interferometry by means of the two-way representation also recovers an estimate of the pressure Green's function as shown in Fig. 15. Similarly to the retrieval of the velocity Green's function, two-way MDD leaves some spurious events in the pressure field (Fig. 15b) that are suppressed in its directionally constrained counterpart (Fig. 15c).

To further study the role of directionality constraints on two-way MDD, Fig. 16 shows the eigenvalues of the three different PSFs for each frequency. While almost half of the most significant PSF singular values for two-way MDD (Fig. 16b) are very similar to those of one-way MDD (Fig. 16a) and the remaining half dramatically drop towards zero, the role of the constraint on directionally of the sought Green's functions becomes evident in Fig. 16(c). The null (or very small) singular values of the two-way PSF are increased in magnitude while the large singular values are almost unchanged. Since conditioning depends on the magnitude of the small singular values compared to the largest, this is clearly improved by the added constraints.

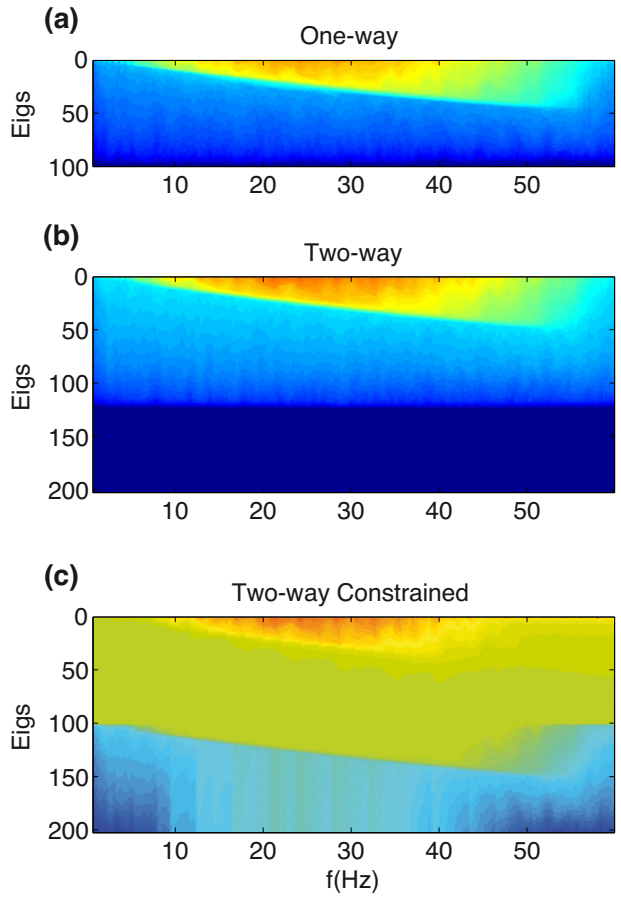

Figure 16. Singular values at each frequency for appropriate PSF matrices in each of the following cases for the configuration in Fig. 11a. (a) One-way MDD (matrix $\mathbf{\Gamma}^{-}_{\mathbf{ow}}$), (b) two-way MDD (matrix $\mathbf{\Gamma}_{\mathbf{tw}}$) and (c) two-way directionally constrained MDD (matrix $\mathbf{\Gamma}_{\mathbf{tw}} + \lambda^2_{D_p}(\mathbf{D}^{+}_{\mathbf{p}})^H\mathbf{D}^{+}_{\mathbf{p}} + \lambda^2_{D_v}(\mathbf{D}^{+}_{\mathbf{v}})^H\mathbf{D}^{+}_{\mathbf{v}}$) with $\lambda^2_{D_p} = \lambda^2_{D_v} = 10$.

Marine streamer virtual dipole sources

In our final example we apply one- and two-way seismic interferometry by MDD to marine streamer type data. Data are modelled an array of 126 sources with spacing $x_s = 8$ m deployed just below the water surface and 101 dual receivers spaced at $x_r = 8$ m at 25 m depth inside the water column (Fig. 17a). We focus on the estimate of Green's functions from virtual dipole sources at locations of particle velocity receivers along the streamer cable, using only monopolar real sources during acquisition since dipole sources are not readily available in many surveys. We only show the velocity response from a virtual horizontal dipole source, but estimates of similar quality have been obtained for the pressure and velocity wavefield emitted by a vertical dipole virtual source. The acquisition geometry is shown in Fig. 17 together with the pressure data (Fig. 17c) acquired from a monopole source at location $x = 0$ m, while (Fig. 17b) depicts the acquisition scenario assumed in this example: a streamer cable is towed behind a source with minimum offset (the distance between the source and the first receiver) of 32 m, and a split-spread acquisition is generated by traversing the same line twice in opposite directions.

van der Neut *et al.* (2012) have recently used seismic interferometry by MDD to remove free surface multiples from streamer data. The main challenge for this type of acquisition is the requirement to include information at near-offsets, which are generally not recorded but are fundamental to be able to invert for the PSF effects. This problem has been overcome by interpolation of the near-offset gap, for instance by using projection on convex sets (Kabir & Verschuur 1995), or by direct arrival prediction based on source near-field hydrophone recordings (Majdanski *et al.* 2011). Here three different strategies are compared, differing in terms of accuracy of the estimate and computational cost:

(1) Near-offset missing traces are interpolated from the available data as in van der Neut *et al.* (2012).
(2) The nearest offset available trace is simply replicated to all of the nearer-offset missing traces.
(3) Near-offset missing traces are set to zero.

In scenario 1, while the interaction of free-surface multiples in the data constructs many spurious arrivals in the cross-correlation estimate (Fig. 18b), both one-way MDD (Fig. 18c) and two-way MDD as in eq. (12) (Fig. 18d) provide a good approximation of the true response in Fig. 18(a). Note especially how the correct radiation pattern of a horizontal dipole source is recovered. In this idealized marine scenario the one-way MDD results produce fewer spurious events before the first arrival. However, when the low wavenumber components—mostly contained in the near-offset (missing) data—are not included correctly (scenarios 2 and 3), the forward problem is not well defined and the deconvolution process is not as successful as with full source coverage in inverting the effect of the PSF (Fig. 19) and hence of the free-surface. In scenario 2, two-way MDD produces fewer later-arriving spurious multiples, and in scenario 3 it is unclear which performs best.

These three different scenarios are further analyzed using the so-called resolution matrix of one-way MDD [$\delta^{-}_{\mathbf{ow}} = \left(\mathbf{\Gamma}^{-}_{\mathbf{ow}}\right)^{\dagger}\mathbf{\Gamma}^{-}_{\mathbf{ow}}$], which is diagnostic of the quality of the MDD process. In the ideal case when the boundary ∂D_R is covered by a dense line of receivers and when there is a densely-sampled source line, the one-way resolution matrix should be $\delta^{-}_{\mathbf{ow}} \rightarrow \mathbf{I}$ for all ω. As shown in Fig. 20 for a single frequency $f = 20$ Hz, the resolution matrices constructed from full data (scenario 1) approaches an identity while those corresponding to replicated (scenario 2) or missing (scenario 3) near-offset traces deviate markedly from the ideal situation of identity matrices, showing both spurious off-diagonal energy and non uniform energy along the diagonal. Since near-offset information is a fundamental part of the data, the forward problem is not well defined when they are not available and, as a consequence, the PSF can not be inverted successfully by MDD.

DISCUSSION

Directional wavefield decomposition is a method that is used frequently in seismic processing to separate events of interest from others that are considered as noise and which affect the interpretability of the data (see Appendix A for a review on wavefield decomposition). However, the requirement of (accurate) knowledge of medium properties along a densely and uniformly sampled receiver array, together with assumptions that the medium properties vary slowly along the receiver array and that the recorded velocity field is a measure of true ground motion (so-called vector fidelity – Norris *et al.* 2006) are not always fulfilled. Moreover, the decomposition matrices in eqs (A3) and (A4) are unstable because of singularities near the critical angle (van der Neut & Herrmann 2013). This introduces errors in the estimates of the decomposed fields that can propagate through the multidimensional inversion process and deteriorate the interferometric estimates.

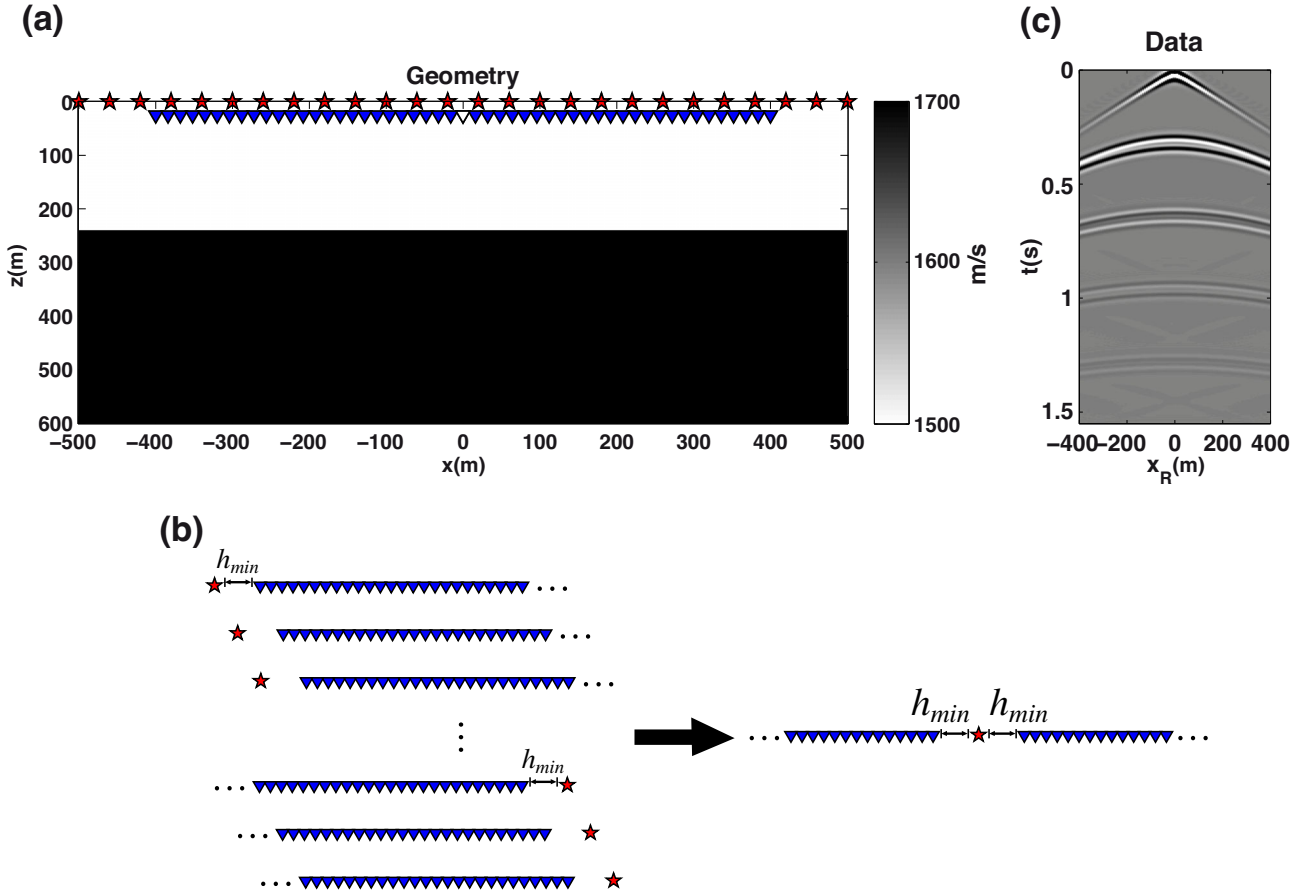

Figure 17. Configuration for streamer virtual dipole estimate. (a) Velocity model together with sources (red stars) situated just below the top surface, and receivers (blue triangles) and virtual source (white triangle) at 25 m depth. (b) Acquisition scenario: a streamer cable of length 1 km is towed behind a source with minimum offset of $h_{\min} = 32$ m and a split-spread acquisition is generated by traversing the same line twice in opposite directions. (c) Recorded pressure data from the source at $x_S = 0$ m.

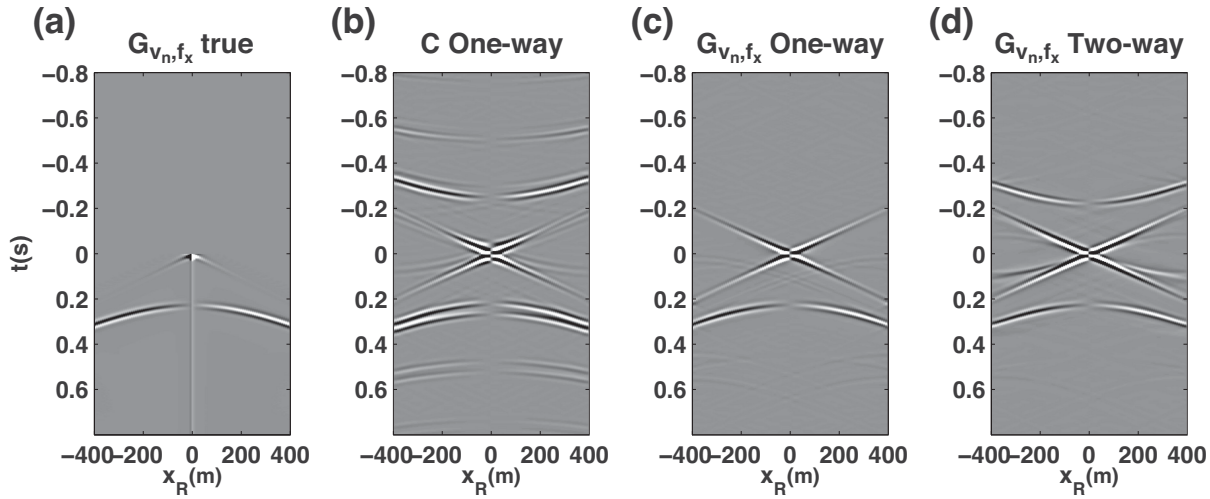

Figure 18. Velocity Green's function from a virtual horizontal dipole source for the configuration in Fig. 17a. (a) Modelled response, and solutions from (b) one-way cross-correlation, (c) one-way MDD and (d) two-way MDD in acquisition scenario 1 (see text).

The ability to implement seismic interferometry by MDD using full (pressure and velocity) fields rather than directionally decomposed fields is beneficial in that the knowledge of medium properties is no longer required (unless directional constraints are used). The decomposition is also directly embedded inside the regularized inverse problem leading to higher fidelity in the reconstruction around the critical angle, as similarly shown by van der Neut and Herrmann (2013) in their wavefield separation via sparsity-promoting inversion. Furthermore, the two-way MDD approach is useful in situations where one or more of the other requirements of wavefield

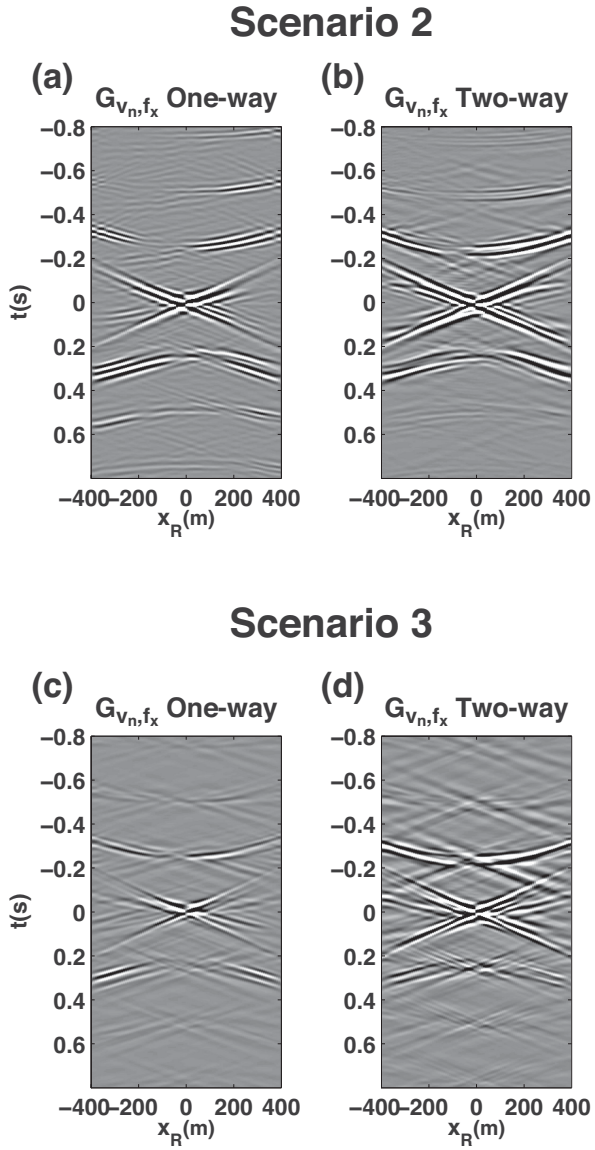

Figure 19. Velocity Green's function from a virtual horizontal dipole source for the configuration in Fig. 11a. (a) and (c) one-way MDD, (b) and (d) two-way MDD in the acquisition scenarios 2 and 3, respectively.

separation are not satisfied. A first encouraging result is shown in Fig. 21 where two-way MDD performs very well even though the receiver array intersects a sudden velocity change (hence the above requirement of slowly-varying properties is not fulfilled). A detailed comparison of our approach with one-way MDD in situations where assumptions of frequency-wavenumber wavefield decomposition are not fulfilled (i.e. medium parameter along the receiver array are not uniquely defined) is however beyond the scope of this paper.

As a consequence of including velocity recordings in the two-way MDD equations, the dimension of the PSF doubles with respect to that of one-way MDD. The effect of this is two-fold: the inversion of the PSF is more computationally expensive for two-way than one-way MDD, and the inverse problem is also generally more poorly conditioned. However, if the inversion of the two-way PSF is performed taking advantage of its structure (a matrix that partitions into block form), two matrices of dimensions $N_R \times N_R$ need to be inverted **(**see Press *et al.* 2002 – p. 77**)** rather than the full matrix of dimension $(2N_R \times 2N_R)$, making the computational cost of two-way MDD only twice that of one-way MDD. Moreover, additional constraints on the solution norm and the directivity of the retrieved Green's functions have been shown to be beneficial to regularize the inverse problem. As an alternative, if two-way MDD was solved in the time-domain as done by van der Neut & Herrmann (2013) for one-way MDD, we could also design a constraint that ensures the acausual solution of the problem to go to zero. While the time-domain inversion is computationally more intensive, an advantage of this regularization term with respect to our directional constraint is that no information about the medium parameters would be required.

Two-way MDD not only redatums the recorded data closer to the imaging target by removing some of the unwanted energy (e.g. free-surface multiples, effect of complex overburden), but also provides estimates of both pressure and particle velocity virtual fields without compromising the vector-acoustic nature of the recorded data. As a consequence, vector-acoustic migration algorithms that take advantage of directionality information contained in the velocity fields (El Yadari & Hou 2013; Fleury & Vasconcelos 2013; Vasconcelos 2013; Amundsen & Robertsson 2014; El Yadari 2015**)** can be applied not only to the original recorded data but also to the virtual data, meaning that MDD redatuming and directional migration could be combined together for more accurate imaging of the target of interest.

In addition, estimates of virtual dipole sources can be produced from velocity recordings. These additional fields could aid reconstruction techniques (for example, interpolation of aliased wavefields in the crossline direction – Vassallo *et al.* 2010**)** as well as imaging algorithms, which could ultimately benefit from the directivity of dual sources in a similar way to that of dual receivers (Fleury & Vasconcelos 2013; Vasconcelos 2013). While we have shown that such virtual sources could readily be created by using MDD in boreholes or using ocean-bottom data, the quality of their Green's function estimates using current standard streamer data with a near-offset gap (even if we do two passes to provide split-spread data) depends strongly on the quality of interpolation of the missing traces.

CONCLUSION

Seismic interferometry by MDD has been formulated using a two-way representation theorem of convolution-type. This form of interferometry simultaneously estimates pressure and velocity virtual responses deprived of the effect of the overburden without requiring a preliminary up/down wavefield separation of the recorded data. However, since the underlying representation is valid for any choice of boundary conditions at the receiver boundary, and for any medium parameters outside of the receiver boundary in the Green's functions wave state, the solution obtained depends on the choice of the minimization criterion and regularization employed. A regularized least-squares solution has been shown to improve the results of interferometry by cross-correlation, and generally to produce estimates of similar quality to those obtained by one-way MDD. In the special case of a receiver array sitting on an interface, as in our example of ocean-bottom multiple suppression, spurious energy is not completely suppressed by unconstrained two-way MDD and additional constraints on the directionality of the reconstructed fields can be added to improve the interferometric estimates by recasting and solving two-way MDD in the frequency–wavenumber domain. Finally, when dual recordings are available, not only estimates of

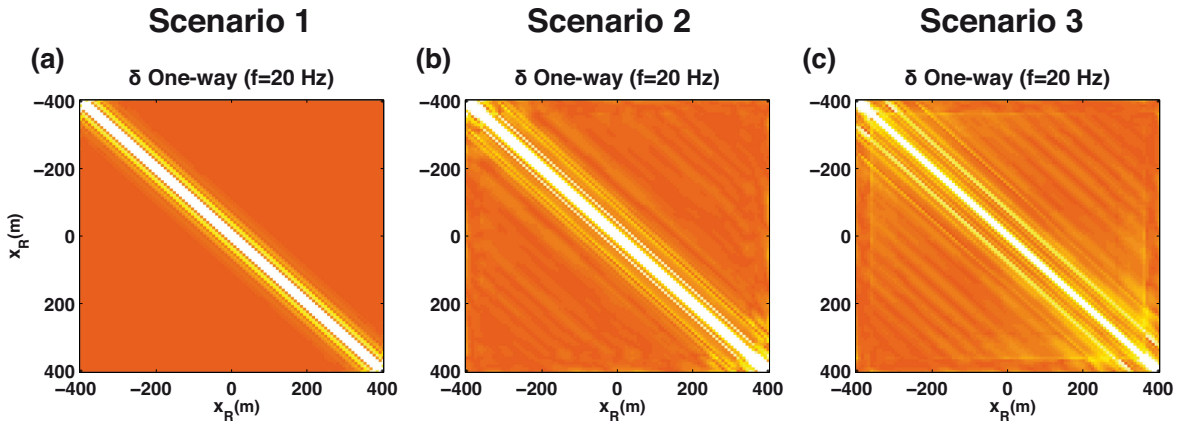

Figure 20. Resolution matrices at $f = 20$ Hz for the configuration in Fig. 11a, for (a) scenario 1, (b) scenario 2 and (c) scenario 3.

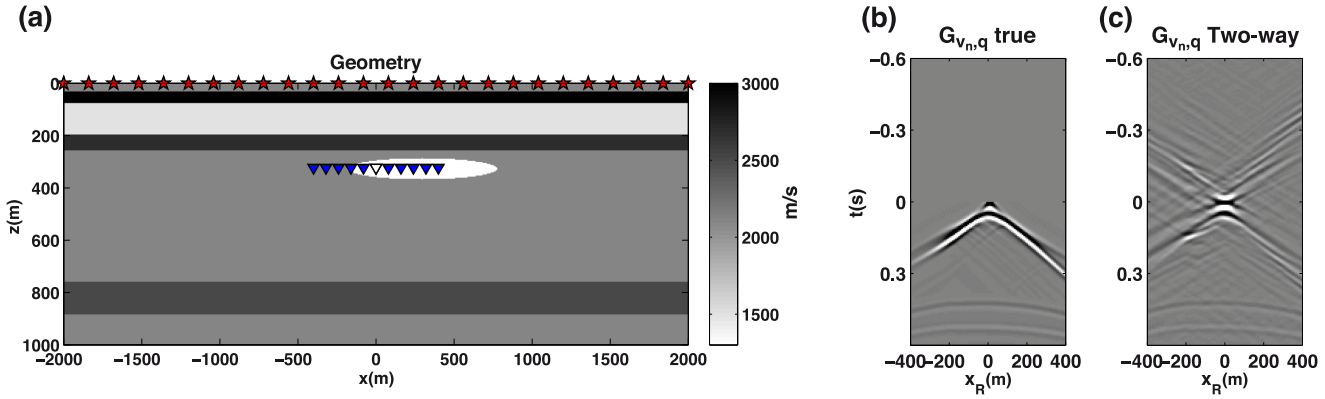

Figure 21. (a) Configuration for borehole redatuming with receivers (blue triangles) in a well crossing a gas cloud at depth $z_R = 328$ m. The virtual source (white triangle) is also located inside the gas cloud and sources (red stars) are situated at the earth's surface. Velocity Green's function from a virtual monopole source, (b) modelled response and solution from (c) two-way MDD. An estimate of similar quality is produced for the pressure Green's function from a virtual monopole source.

velocity (and pressure) Green's functions from virtual monopole sources can be obtained via MDD, but also dipole sources can be excited virtually by deconvolving modifications of one- and two-way representation theorems in a multidimensional fashion. Thus Green's functions from dipolar sources can be estimated using data from only standard marine pressure sources.

ACKNOWLEDGEMENTS

The authors thank the Edinburgh Interferometry Project (EIP) sponsors (ConocoPhillips, Schlumberger Gould Research, Statoil and Total) for supporting this research. We also thank Ivan Vasconcelos, David Halliday and Carlos da Costa for valuable discussions. The constructive comments of editor Rene-Edouard Plessix, Joost van der Neut and an anonymous reviewer have helped to improve this paper.

REFERENCES

Amundsen, L., 1993. Wavenumber-based filtering of marine point-source data, *Geophysics,* **58,** 1335–1348.

Amundsen, L., 2001. Elimination of free-surface related multiples without need of the source wavelet, *Geophysics,* **66**(1), 327–341.

Amundsen, L. & Reitan, A., 1995. Decomposition of multicomponent seafloor data into upgoing and downgoing *P*- and *S*-waves, *Geophysics,* **60,** 563–572.

Amundsen, L. & Robertsson, J.O.A., 2014. Wave equation processing using finite-difference propagators, Part 1: wavefield dissection and imaging of marine multicomponent seismic data, *Geophysics,* **79,** T287–T300.

Bakulin, A. & Calvert, R., 2006. The virtual source method: theory and case study, *Geophysics,* **71,** SI139–SI150.

Bellezza, C. & Poletto, F., 2014. Multidimensional deconvolution and processing of seismic-interferometry Artic data, *Geophysics,* **79**(3), WA25–WA38.

Campillo, M. & Paul, A., 2003. Long-range correlations from the diffuse seismic coda, *Science,* **299,** 547–549.

Curtis, A., Gerstoft, P., Sato, H., Snieder, R. & Wapenaar, K., 2006. Seismic interferometry—turning noise into signal, *Leading Edge,* **25**(9), 1082–1092.

Draganov, D., Wapenaar, K. & Thorbecke, J., 2006. Seismic interferometry: reconstructing the Earth's reflection response, *Geophysics,* **71**(4), SI61, doi:10.1190/1.2209947.

El Yadari, N., 2015. True-amplitude vector-acoustic imaging: application of Gaussian beams, *Geophysics,* **80**(1), S43–S54.

El Yadari, N. & Hou, S., 2013. Vector-acoustic Kirchhoff Migration and its mirror extension—theory and examples, in *Proceedings of the 75th EAGE Conference & Exhibition Extended Abstracts*.

Fleury, C. & Vasconcelos, I., 2013. Adjoint-state reverse-time migration of 4C data: finite-frequency map migration for marine seismic imaging, *Geophysics,* **78**(2), WA159–WA172.

Fokkema, J. & van den Berg, P., 1993. *Seismic Applications of Acoustic Reciprocity,* Elsevier Science.

Forghani, F. & Snieder, R., 2010. Underestimation of body waves and feasibility of surface-wave reconstruction by seismic interferometry, *Leading Edge,* **29**(7), 790–794.

Galetti, E. & Curtis, A., 2012. Generalised receiver functions and seismic interferometry, *Tectonophysics,* **532–535,** 1–26.
Grimbergen, J.L.T., Dessing, F.J. & Wapenaar, K., 1998. Modal expansion of one-way operators in laterally varying media, *Geophysics,* **63,** 995–1005.
Kabir, M.M.N. & Verschuur, D.J., 1995. Restoration of missing offsets by parabolic Radon transform, *Geophys. Prospect.,* **43,** 347–368.
Majdanski, M., Kostov, C., Kragh, E., Moore, I., Thompson, M. & Mispel, J., 2011. Attenuation of free-surface multiples by up/down deconvolution for marine towed-streamer data, *Geophysics,* **76**(6), 129–138.
Mehta, K., Bakulin, A., Sheiman, J., Calvert, R. & Snieder, R., 2007. Improving the virtual source method by wavefield separation, *Geophysics,* **72,** V79–V86.
Menke, W., 1989. *Geophysical Data Analysis,* Academic Press.
Minato, S., Matsuoka, T., Tsuji, T., Draganov, D., Hunziker, J. & Wapenaar, K., 2011. Seismic interferometry using multidimensional deconvolution and crosscorrelation for crosswell seismic reflection data without borehole sources, *Geophysics,* **76**(1), SA19–SA34.
Nakata, N., Snieder, R. & Behm, M., 2014. Body-wave interferometry using regional earthquakes with multidimensional deconvolution after wavefield decomposition at free surface, *Geophys. J. Int.,* **199,** 1125–1137.
Norris, M., Johnson, M. & Walsch, M., 2006. OBC signal fidelity, *Geophys. Prospect.,* **54,** 793–815.
Press, W.H., Flannery, B.P., Teukolsky, S.A. & Vetterling, W.T., 2002. *Numerical Recipes in C: The Art of Scientific Computing,* 2nd edn, Cambridge Univ. Press.
Ravasi, M. & Curtis, A., 2013. Elastic imaging with exact wavefield extrapolation for application to ocean bottom 4C seismic data, *Geophysics,* **78,** S265–S284.
Ruigrok, E., Campman, X., Draganov, D. & Wapenaar, K., 2010. High-resolution lithospheric imaging with seismic interferometry, *Geophys. J. Int.,* **183**(1), 339–357.
Schalkwijk, K.M., Wapenaar, C.P.A. & Verschuur, D.J., 2003. Adaptive decomposition of multicomponent ocean-bottom seismic data into downgoing and upgoing *P*- and *S*-waves, *Geophysics,* **68,** 1091–1102.
Schuster, G.T., 2009. *Seismic Interferometry,* Cambridge Univ. Press
Schuster, G.T., Yu, J., Sheng, J. & Rickett, J., 2004. Interferometric/daylight seismic imaging, *Geophys. J. Int.,* **157**(2), 838–852.
Slob, E., Draganov, D. & Wapenaar, K., 2007. Interferometric electromagnetic Green's functions representations using propagation invariants, *Geophys. J. Int.,* **169**(1), 60–80.
Snieder, R., 2006. Retrieving the Green's function of the diffusion equation from the response to a random forcing, *Phys. Rev. E,* **74,** 046620, doi:10.1103/PhysRevE.74.046620.
Sommerfeld, A., 1954. *Optics,* Academic Press.
van Dalen, K., Wapenaar, K. & Halliday, D., 2014. Surface wave retrieval in layered media using seismic interferometry by multidimensional deconvolution, *Geophys. J. Int.,* **196,** 230–242.
van der Neut, J., Frijlink, M. & van Borselen, R., 2012. Data matching for free-surface multiple attenuation by multidimensional deconvolution, *Geophys. J. Int.,* **191,** 743–750.
Van der Neut, J. & Herrmann, F., 2013. Interferometric redatuming by sparse inversion, *Geophys. J. Int.,* **192,** 666–670.
van der Neut, J., Thorbecke, J., Mehta, K., Slob, E. & Wapenaar, K., 2011a. Controlled-source interferometric redatuming by crosscorrelation and multidimensional deconvolution in elastic media, *Geophysics,* **76**(4), SA63–SA76.
van der Neut, J., Tatanova, M., Thorbecke, J., Slob, E. & Wapenaar, K., 2011b. Deghosting, demultiple and deblurring in controlled-source seismic interferometry, *Int. J. Geophys.,* **2011,** 870819.
van Manen, D.-J., Curtis, A. & Robertsson, J.O.A., 2006. Interferometric modeling of wave propagation in inhomogeneous elastic media using time reversal and reciprocity, *Geophysics,* **71**(4), SI47–SI60.
van Manen, D.-J., Robertsson, J.O.A. & Curtis, A., 2005. Modeling of wave propagation in inhomogeneous media, *Phys. Rev. Lett.,* **94**(16), doi:10.1103/PhysRevLett.94.164301.
Vasconcelos, I., 2013. Source-receiver reverse-time imaging of dual-source, vector-acoustic seismic data, *Geophysics,* **78**(2), WA147–WA158.
Vasconcelos, I. & Rickett, J., 2013. Broadband extended images by joint inversion of multiple blended wavefields, *Geophysics,* **78,** WA147–WA158.
Vasconcelos, I., Ravasi, M. & van der Neut, J., 2014. An interferometry-based, subsurface-domain objective function for waveform inversion, in *Proceeding of the 76th EAGE Conference & Exhibition Extended Abstracts,* doi:10.3997/2214-4609.20141090.
Vassallo, M., Özbek, A., Özdemir, K. & Eggenberger, K., 2010. Crossline wavefield reconstruction from multicomponent streamer data. Part 1: multichannel interpolation by matching pursuit (MIMAP) using pressure and its crossline gradient, *Geophysics,* **75,** WB53, doi:10.1190/1.3496958.
Wapenaar, K., 2004. Retrieving the elastodynamic green's function of an arbitrary inhomogeneous medium by cross correlation, *Phys. Rev. Lett.,* **93**(25), 1–4.
Wapenaar, K., 2006. Green's function retrieval by crosscorrelation in case of one-sided illumination, *Geophys. Res. Lett.,* **33,** L19304-1–L19304-6.
Wapenaar, K. & Berkhout, A., 1989. *Elastic Wave Field Extrapolation: Redatuming of Single- and Multi-Component Seismic Data,* Elsevier Science Publ. Co., Inc.
Wapenaar, K. & Fokkema, J., 2006. Green's function representations for seismic interferometry, *Geophysics,* **71**(4), SI33–SI46.
Wapenaar, K. & van der Neut, J., 2010. A representation for Green's function retrieval by multidimensional deconvolution, *J. acoust. Soc. Am.,* **128**(6), EL366–EL371.
Wapenaar, K., Slob, E. & Snieder, R., 2008a. Seismic and electromagnetic controlled-source interferometry in dissipative media, *Geophys. Prospect.,* **56,** 419–434.
Wapenaar, K., van der Neut, J. & Ruigrok, E., 2008b. Passive seismic interferometry by multidimensional deconvolution, *Geophysics,* **73,** A51–A56.
Wapenaar, K., Draganov, D., Snieder, R., Campman, X. & Verdel, A., 2010a. Tutorial on seismic interferometry. Part 1: basic principles and applications, *Geophysics,* **75,** A195–A209.
Wapenaar, K., Slob, E., Snieder, R. & Curtis, A., 2010b. Tutorial on seismic interferometry. Part 2: underlying theory, *Geophysics,* **75,** A211–A227.
Wapenaar, K., van der Neut, J., Ruigrok, E., Draganov, D., Hunziker, J., Slob, E., Thorbecke, J. & Snieder, R., 2011. Seismic interferometry by crosscorrelation and by multi-dimensional deconvolution: a systematic comparison, *Geophys. J. Int.,* **185,** 1335–1364.
Weaver, R.L. & Lobkis, O.I., 2001. Ultrasonics without a source: thermal fluctuation correlations at MHz frequencies, *Phys. Rev. Lett.,* **87**(13), 134301, doi:10.1103/PhysRevLett.87.134301.
Weglein, A.B., Mayhan, J.D., Amundsen, L., Liang, H., Wu, J., Tang, L., Luo, Y. & Fu, Q., 2013. Green's theorem de-ghosting algorithms in k, ω (e.g., P-Vz de-ghosting) as a special case of x, ω algorithms (based on Green's theorem) with: (1) significant practical advantages and disadvantages of algorithms in each domain, and (2) a new message, implication and opportunity for marine towed streamer, ocean bottom and onshore acquisition and applications, *J. Seismic Explor.,* **22,** 389–412.
Ziolkowski, A., Taylor, D.B. & Johnston, R.G.K., 1999. Marine seismic wavefield measurement to remove sea surface multiples, *Geophys. Prospect.,* **47,** 6841–870.

APPENDIX A: UP/DOWN WAVEFIELD SEPARATION

It has long been recognized that seismic recordings can be split into in- and out-going waves with respect to a chosen boundary line ∂D_R (see Fig. 1)

$$p = p^+ + p^-, \qquad v_i = v_i^+ + v_i^-, \tag{A1}$$

where p indicates the pressure recording and v_i the particle velocity recording along the i-th direction, while superscripts + and – refer to in- and outgoing constituents, respectively. In addition, the normal

component of the particle velocity v_n is uniquely related to the normal derivative of pressure via the equation of motion

$$\frac{\partial p}{\partial n} = -\rho j\omega v_n. \tag{A2}$$

The approach used in this paper to obtain decomposed fields in the special case of a horizontal boundary ∂D_{R}, where in- and outgoing constituents are generally referred as downgoing and upgoing constituents, operates in the frequency–wavenumber (fk) domain. Up- and downgoing components of pressure and normal particle velocity are in fact related to the full pressure and the normal particle velocity recordings by the matrix equations (Wapenaar & Berkhout 1989; Amundsen 1993; Fokkema & Van den Berg 1993)

$$\begin{bmatrix} p^+ \\ p^- \end{bmatrix} = \frac{1}{2}\begin{bmatrix} 1 & \xi \\ 1 & -\xi \end{bmatrix}\begin{bmatrix} p \\ v_n \end{bmatrix} \tag{A3}$$

$$\begin{bmatrix} v_n^+ \\ v_n^- \end{bmatrix} = \frac{1}{2}\begin{bmatrix} 1 & 1/\xi \\ 1 & -1/\xi \end{bmatrix}\begin{bmatrix} p \\ v_n \end{bmatrix}, \tag{A4}$$

where $\xi(k_x) = \rho\frac{\omega}{k_z(k_x)}$ is the so-called obliquity factor, $k_z(k_x) = \sqrt{\left(\frac{\omega}{c}\right)^2 - k_x^2}$ is the vertical wavenumber, k_x is the horizontal wavenumber, ρ and c are the density and the velocity at the receiver level, respectively. If we are only interested in obtaining the downgoing constituents of both pressure and particle velocity as in the main text, we can define the downgoing two decomposition vectors $\mathbf{D}_{\mathbf{p}}^+, \mathbf{D}_{\mathbf{v}}^+$ (in eq. 14) by extracting the first line of the decomposition matrices in eqs (A3) and (A4).

Requirements to be fulfilled for an accurate up/down wavefield separation in the frequency–wavenumber domain (Weglein *et al.* 2013) are (i) accurate knowledge of medium properties (ρ, c) at the receiver array, (ii) a horizontally layered (or slowly laterally varying) medium along the receiver array, (iii) horizontal (or, at least, flat) boundary ∂D_{R} where fk transform and separation is carried out and (iv) adequate sampling and aperture to perform an fk transform. The number of assumptions can be reduced if more accurate separation techniques are used, such that wavefield decomposition can be performed in the frequency–space domain (Grimbergen *et al.* 1998; Wapenaar *et al.* 2008a; Weglein *et al.* 2013) or by means of finite-difference injection (Ravasi & Curtis 2013; Vasconcelos 2013; Amundsen & Robertsson 2014). The latter method, for example, can accommodate an arbitrary measurement surface geometry and does not require an estimate of the local medium parameters.

APPENDIX B: ANTICAUSAL SOLUTIONS OF TWO-WAY MDD

The convolution-type representation in eq. (1) contains causal Green's functions $G_{p,q}$ and $G_{v_n,q}$, and likewise we expect to retrieve only causal (one-sided) Green's functions by inverting eq. (10) by means of MDD (eq. 12).

However, a correlation-type representation can also be written to relate the fields in Fig. 1 (Slob *et al.* 2007)

$$p(\mathbf{x}_{vs}, \mathbf{x}_s, \omega) = \oint_{\partial D_R} p(\mathbf{x}_r, \mathbf{x}_s, \omega)G^*_{v_n,q}(\mathbf{x}_r, \mathbf{x}_{vs}, \omega) + v_n(\mathbf{x}_r, \mathbf{x}_s, \omega)G^*_{p,q}(\mathbf{x}_r, \mathbf{x}_{vs}, \omega)\,\mathrm{d}\mathbf{x}_r, \tag{B1}$$

where an enclosing boundary ∂D_{R} is here required since radiation conditions can not be applied to eliminate the contribution of the half-sphere that would close the boundary. In practice, the quantities along the lower boundary are not available and for this reason we usually discard such contributions. Note however that this approximation is justified only if the medium is strongly reflective below $\mathbf{x}_{vs}$ (Wapenaar 2006).

Eq. (B1) can then be converted into matrix form using the same quantities defined in eq. (10):

$$\mathbf{p} = \begin{bmatrix} \bar{\mathbf{p}} & \bar{\mathbf{v}} \end{bmatrix}\begin{bmatrix} \mathbf{G}_{\mathbf{v}}^* \\ \mathbf{G}_{\mathbf{p}}^* \end{bmatrix} = \begin{bmatrix} \bar{\mathbf{p}} & -\bar{\mathbf{v}} \end{bmatrix}\begin{bmatrix} \mathbf{G}_{\mathbf{v}}^* \\ -\mathbf{G}_{\mathbf{p}}^* \end{bmatrix} \Leftrightarrow \mathbf{p} = \mathbf{d}\mathbf{G}_{\mathbf{tw}}^* \tag{B2}$$

and eqs (10) and (B2) are combined to obtain

$$\mathbf{p} = \mathbf{d}\left(\alpha\mathbf{G}_{\mathbf{tw}} + \beta\mathbf{G}_{\mathbf{tw}}^*\right), \tag{B3}$$

where α and β are constants such that $\forall\alpha, \beta$: $\alpha + \beta = 1$. Thus we see why solving two-way MDD in fact provides both causal and anticausal Green's functions, since in the time domain $\mathbf{G}_{\mathbf{tw}}^*$ is the time-reverse of $\mathbf{G}_{\mathbf{tw}}$. Eqs (10) and (B2) also show the reason for the different polarity of the anticausal pressure Green's functions in Figs 8 and 15. The term $\mathbf{G}_{\mathbf{p}}$ comes with a plus sign in the Green's function vector $\mathbf{G}_{\mathbf{tw}}$ in eq. (10) and with minus sign in the Green's function vector $\mathbf{G}_{\mathbf{tw}}^*$ in eq. (B2).

We now show that when we solve two-way MDD in a regularized sense by finding the solution at minimum norm (eq. 11), such a regularization term is responsible for choosing a specific pair of α, β, namely $\alpha = \beta = 0.5$. In the time domain, we first define the norm of the solution in eq. (B3)

$$J_{\mathrm{G}} = \left\|\alpha\mathbf{G}_{\mathbf{tw}}(t) + \beta\mathbf{G}_{\mathbf{tw}}(-t)\right\|_2 = \left(\alpha\mathbf{G}_{\mathbf{tw}}(t), \alpha\mathbf{G}_{\mathbf{tw}}(t)\right) + \left(\beta\mathbf{G}_{\mathbf{tw}}(-t), \beta\mathbf{G}_{\mathbf{tw}}(-t)\right) + 2\left(\alpha\mathbf{G}_{\mathbf{tw}}(t), \beta\mathbf{G}_{\mathbf{tw}}(-t)\right), \tag{B4}$$

where (,) represents the scalar product that here represents the product of each of the time samples, integrated over time. By noting that $\mathbf{G}_{\mathbf{tw}}(t)$ is causal while $\mathbf{G}_{\mathbf{tw}}(-t)$ is anticausal, their scalar products $(\mathbf{G}_{\mathbf{tw}}(t),\ \mathbf{G}_{\mathbf{tw}}(-t))$ and $(\mathbf{G}_{\mathbf{tw}}(-t),\ \mathbf{G}_{\mathbf{tw}}(t))$ are both zeros. Moreover, since the two Green's functions have the same energy $((\mathbf{G}_{\mathbf{tw}}(t), \mathbf{G}_{\mathbf{tw}}(t)) = (\mathbf{G}_{\mathbf{tw}}(-t), \mathbf{G}_{\mathbf{tw}}(-t)) = k_{tw})$ we obtain

$$J_{\mathrm{G}} = k_{tw}\left(\alpha^2 + \beta^2\right). \tag{B5}$$

Using the fact that $\alpha = 1 - \beta$ the value of β that minimizes J_{G} is 0.5 and so the value of α. The causal and anticausal solutions obtained by solving two-way MDD have indeed the same energy as shown in Figs 7, 8, and 14.

We also convert eq. (B1) into a representation theorem for virtual dipole sources. By multiplying each side of the equation by the operator that transforms pressure fields into particle velocity fields [i.e. $-(j\omega\rho)^{-1}\partial_i$] at the virtual source location, we obtain

$$v_i(\mathbf{x}_{vs}, \mathbf{x}_s, \omega) = \oint_{\partial D_R} -p(\mathbf{x}_r, \mathbf{x}_s, \omega)G^*_{v_n,f_i}(\mathbf{x}_r, \mathbf{x}_{vs}, \omega) - v_n(\mathbf{x}_r, \mathbf{x}_s, \omega)G^*_{p,f_i}(\mathbf{x}_r, \mathbf{x}_{vs}, \omega)\,\mathrm{d}\mathbf{x}_r. \tag{B6}$$

By comparing eq. (B6) with eq. (18) we can thus explain the change in polarity in the anticausal estimate of the velocity Green's function from a virtual dipole source (see Figs 9 and 18). On the other hand, the causual and anticausal estimates of the pressure Green's function from a virtual dipole share the same polarity (see Fig. 10). The term G_{v_n,f_i} in fact comes with a plus sign in eq. (18) and with minus sign in eq. (B6), while the term G_{p,f_i} has a minus sign in both equations.

Finally, it is interesting to note that by adding directional constraints that annihilate the downgoing energy of the estimated Green's functions as done in eq. (16), the anticausal component of the estimated Green's functions goes to zero. To explain this phenomenon, we first convert the two-way correlation-type theorem (eq. B1) into its one-way (directional) counterpart. Conversely

to the convolution-type theorem, the two products between in- and out-going terms at the stationary receiver locations have opposite contributions that cancel (Wapenaar & Berkhout 1989). Consequently, eq. (B1) can be written as

$$\begin{aligned} p(\mathbf{x}_{vs}, \mathbf{x}_s, \omega) = &\int_{\partial D_R} p^-(\mathbf{x}_r, \mathbf{x}_s, \omega) G^{-*}_{v_n,q}(\mathbf{x}_r, \mathbf{x}_{vs}, \omega) \\ &+ p^+(\mathbf{x}_r, \mathbf{x}_s, \omega) G^{+*}_{v_n,q}(\mathbf{x}_r, \mathbf{x}_{vs}, \omega)\, \mathrm{d}\mathbf{x}_r \\ + &\int_{\partial D_R} v_n^-(\mathbf{x}_r, \mathbf{x}_s, \omega) G^{-*}_{p,q}(\mathbf{x}_r, \mathbf{x}_{vs}, \omega) \\ &+ v_n^+(\mathbf{x}_r, \mathbf{x}_s, \omega) G^{+*}_{p,q}(\mathbf{x}_r, \mathbf{x}_{vs}, \omega)\, \mathrm{d}\mathbf{x}_r. \end{aligned} \tag{B7}$$

We note that by invoking the directional constraints (i.e. $G^+_{v_n,q} = G^+_{p,q} = 0$), we are implicitly solving the following version of the one-way convolution-theorem

$$\begin{aligned} p(\mathbf{x}_{vs}, \mathbf{x}_s, \omega) = &\int_{\partial D_R} p^+(\mathbf{x}_r, \mathbf{x}_s, \omega) G^{-}_{v_n,q}(\mathbf{x}_r, \mathbf{x}_{vs}, \omega) \\ &- v_n^+(\mathbf{x}_r, \mathbf{x}_s, \omega) G^{-}_{p,q}(\mathbf{x}_r, \mathbf{x}_{vs}, \omega)\, \mathrm{d}\mathbf{x}_r \end{aligned} \tag{B8}$$

or this version of the one-way correlation-theorem

$$\begin{aligned} p(\mathbf{x}_{vs}, \mathbf{x}_s, \omega) = &\int_{\partial D_R} p^-(\mathbf{x}_r, \mathbf{x}_s, \omega) G^{-*}_{v_n,q}(\mathbf{x}_r, \mathbf{x}_{vs}, \omega) \\ &+ v_n^-(\mathbf{x}_r, \mathbf{x}_s, \omega) G^{-*}_{p,q}(\mathbf{x}_r, \mathbf{x}_{vs}, \omega)\, \mathrm{d}\mathbf{x}_r \end{aligned} \tag{B9}$$

which converted into matrix equations, become

$$\mathbf{p} = \begin{bmatrix} \mathbf{p}^+ & -\mathbf{v}^+ \end{bmatrix} \begin{bmatrix} \mathbf{G}^-_{\mathbf{v}} \\ \mathbf{G}^-_{\mathbf{p}} \end{bmatrix} \Leftrightarrow \mathbf{p} = \mathbf{d}^+ \mathbf{G}^-_{\mathbf{tw}} \tag{B10}$$

$$\mathbf{p} = \begin{bmatrix} \mathbf{p}^- & \mathbf{v}^- \end{bmatrix} \begin{bmatrix} \mathbf{G}^{-*}_{\mathbf{v}} \\ \mathbf{G}^{-*}_{\mathbf{p}} \end{bmatrix} \Leftrightarrow \mathbf{p} = \mathbf{d}^- \mathbf{G}^{-*}_{\mathbf{tw}}. \tag{B11}$$

Since the operands $\mathbf{d}^+$ and $\mathbf{d}^-$ in eqs. (B10) and (B11) contain different quantities, the convolution problem (i.e. causal solution) can be solved without leaking energy from the correlation problem (i.e. anticausal solution) by inputting $\mathbf{p}$ and $-\bar{\mathbf{v}}$ together with the directional constraint to the MDD inversion scheme (see, for example, Fig. 14).